Brownian Motion in One-Dimensional Models: Scaling, Universality, and Dispersionless Transport

by

© *Amir Kaffashnia*

Supervisor

Dr. Mykhaylo Evstigneev

A proposal submitted to the School of Graduate Studies

in partial fulfillment of the requirements for the degree of

Doctor of Philosophy

Department of *Physics and Physical Oceanography*

Memorial University of Newfoundland

Summer 2023

St. John's Newfoundland

Abstract

In the studies of Brownian motion, one-dimensional (1D) models play a special role in view of their relative simplicity and also because diffusion in a higher-dimensional space can often be decomposed into independent random motions in the orthogonal directions. In this thesis, we investigate the diffusion behavior of a Brownian particle (BP) within three 1D models: (i) diffusion along a stochastic harmonic oscillator chain (SHOC), (ii) diffusion of a damped BP in a tilted periodic potential, and (iii) free diffusion described by the Langevin equation with velocity-dependent damping. To address the first problem, we invent moving stochastic boundary condition approach, which allows us to simulate a small subset of oscillators in close proximity to the BP, effectively capturing the relevant dynamics. Our investigations have revealed a power law relation between the diffusion coefficient D and temperature T and the existence of dispersionless undamped phases in the BP motion at high temperatures. In the context of the second model, we explore the phenomenon of dispersionless transport of a BP in a tilted periodic potential, which is described in the literature as a broad time interval during which the particle's dispersion appears to be constant. Our findings demonstrate that the dispersion fluctuations within the dispersion plateau hinder accurate determination of D, but these challenges can be remedied by employing an alternative measurement procedure. Moreover, it is evident that the conventional Langevin equation with velocity-independent damping coefficient as used in model (ii) cannot reproduce the nearly undamped ballistic flights observed in various physical systems. Lastly, we focus on establishing an analytical relation between D and T for a BP subject to velocity-dependent damping $\gamma(v)$ and apply it to the case of a monotonically decreasing function $\gamma(v) > 0$. We show that at low temperatures, the D vs. T relation is linear; however, at high temperatures, a non-Einsteinian behavior emerges, similar to the one found within the SHOC diffusion model.

General Summary

The random Brownian movement of particles immersed in a medium with a huge number of atoms is a ubiquitous phenomenon observed in a wide range of physical, chemical, and biological systems, from ultracold atoms in optical traps to proteins in living cells to weather balloons in the atmosphere. Although it has been discussed in physics literature for over a hundred years, it continues to surprise researchers even today by manifesting its counterintuitive facets, such as sub- and superdiffusion and the existence of Lévy flights.

To investigate Brownian motion, Molecular Dynamics (MD) simulations are routinely performed, in which the trajectories of the BP and of many surrounding atoms are computed numerically. Unfortunately, MD is limited by the computational resources required to simulate large-scale systems or long-duration processes. To overcome these limitations, stochastic modeling based on the Langevin equation (LE) offer distinct advantages. However, the LE method also has its limitations, as it neglects microscopic details and interactions which may be crucial in some systems.

In this thesis, our primary objective is to examine the dynamics of a Brownian particle (BP) within three one-dimensional models. Our research in the first model is motivated by the need for new methodologies that can overcome the limitations associated with the aforementioned approaches. To achieve this, we employ the moving stochastic boundary condition to explore Brownian motion on a stochastic harmonic oscillator chain (SHOC). As a result, we are able to probe the BP dynamics on a very long time scales.

We find that, intriguingly, at high temperatures, the BP motion proceeds via long flights, in which the particle travels large distances with an almost constant velocity; during these flights, the particle motion is dispersionless.

The term "dispersionless transport" has been used in the literature in the context of LE simulations of Brownian motion in a tilted periodic potential. This is revisited in the

second model of this thesis. It is shown that the term "dispersionless" in this model is actually a misnomer: the BP in fact undergoes regular diffusion without long flights.

A modification of the standard LE is proposed in the third model, which allows reproducing those flights. An analytical expression for the diffusion coefficient of the BP is obtained and some features of its dynamics resembling those found in the SHOC diffusion model are observed.

Co-authorship Statement

This manuscript-style thesis consists of three papers published in Physical Review E. Each of these papers is a co-authored work by the thesis author, Amir Kaffashnia, and his supervisor, Dr. Mykhaylo Evstigneev:

A. Kaffashnia and M. Evstigneev, "Origin of the dispersionless transport in spite of thermal noise". Phys. Rev. E, 104, 054113, (2021).

A. Kaffashnia and M. Evstigneev, "Scaling and universality in Brownian motion on a stochastic harmonic oscillator chain". Phys. Rev. E, 105, 064134, (2022).

M. Evstigneev and A. Kaffashnia, "Diffusion coefficient scaling of a free Brownian particle with velocity-dependent damping". Phys. Rev. E, 107, 064129, (2023).

In these collaborative efforts, Dr. Evstigneev provided the research topics and Amir Kaffashnia performed numerical and analytical calculations. In the third paper, analytical calculations were performed by Dr. Evstigneev. Both authors participated equally in data analysis and write-up of all three manuscripts.

Acknowledgments

I would like to express my sincere gratitude to my supervisor, Dr. Mykhaylo Evstigneev, for his support, guidance, and expertise during my Ph.D. studies. His mentorship has transcended the academic realm, providing invaluable insights and assistance in various aspects of my personal and professional growth.

I would also like to extend my heartfelt thanks to my wife, Arzu, and my parents for their unwavering support throughout my academic journey. Their encouragement, understanding, and belief in me have been invaluable, and I am truly grateful for their constant presence in my life.

Additionally, I would like to acknowledge the support and resources provided by the Department of Physics and Physical Oceanography at Memorial University of Newfoundland, which have greatly contributed to the successful completion of this thesis.

Contents

List of Figures

Abbreviations

1D	One Dimensional
BP	Brownian Particle
GLE	Generalized Langevin Equation
LE	Langevin Equation
MD	Molecular Dynamics
MSBC	Moving Stochastic Boundary Condition
MSD	Mean Square Displacement
PBC	Periodic Boundary Condition
SBC	Stochastic Boundary Condition
SHOC	Stochastic Harmonic Oscillator Chain

Chapter 1

Introduction

In the introductory chapter we provide an overview of the key topics to be discussed in this thesis. The chapter begins with a historical review of Brownian motion, shedding light on its early observations and subsequent investigations. We then delve into the main modeling approaches, Molecular Dynamics (MD) simulations and stochastic simulations based on the Lagnevin equation. Furthermore, we touch upon the concept of anomalous diffusion. We also explore the intriguing phenomenon of dispersionless transport. Finally, we briefly discuss non-Einsteinian diffusion, offering a glimpse into deviations from the conventional Einstein relation. This chapter sets the foundation for a systematic exploration of these aspects in the subsequent chapters, enabling a deeper understanding of Brownian motion and its complex dynamics.

1.1 Brownian motion: historical overview

The observation of powdered charcoal dispersed on the surface of alcohol under a microscope reveals an intriguing phenomenon of random motion, known as Brownian motion. It is attributed to the collisions between alcohol molecules and the larger charcoal particles.

The initial investigation of this phenomenon dates back to 1785 when Jan Ingenhausz, a renowned Dutch physician credited with the discovery of photosynthesis, observed it for the first time [1]. Subsequently, the systematic study of Brownian motion was carried out by Robert Brown, leading to the nomenclature of this phenomenon as "Brownian motion" in 1828. In the early days of its discovery, the spontaneous movement of particles appeared enigmatic, as the existence of atoms had not been established at that time. The understanding of why Brownian particles (BP) exhibited apparently self-driven motion remained elusive.

It was not until 1905 when Albert Einstein published a seminal paper [2], in which the motion of pollen grains in a liquid was explained as driven by the molecular motion of the surrounding molecules. Einstein's explanation indirectly provided evidence for the existence of atoms and molecules. He mathematically determined the mean square displacement (MSD) of a BP and established its connection to Avogadro's number. This hypothesis was subsequently validated in 1908 by Jean Perrin, who earned the 1926 Nobel Prize in physics for his experimental work on the discontinuous structure of matter and determination of Avogadro's number [1,3].

Since its first theoretical description in 1905, Brownian motion has served as a fundamental example of a random process [4]. Notable contributions were made by William Sutherland [5], Marian Smoluchowski [6], and Paul Langevin [7], who dedicated their research efforts to elucidating the mathematical properties of Brownian motion. Through distinct approaches, they derived an equation governing the probability distribution $P(x,t)$, which describes the position x of a BP at time t given its initial position at the origin. In one dimension, this equation is

$$\frac{\partial P(x,t)}{\partial t} = D\frac{\partial^2 P(x,t)}{\partial x^2} \ . \tag{1.1}$$

The diffusion equation, Eq. (1.1), was initially formulated by Fourier as a description of

heat conduction, implying that the diffusion of probability follows a similar mechanism.

If the particle started at origin, $x(t = 0) = 0$, the initial condition of its probability density is expressed with the help of Dirac delta function: $P(x, 0) = \delta(x)$. With this initial condition, the particle probability density at any time $t > 0$ is given by a Gaussian function

$$P(x,t) = \frac{1}{\sqrt{4\pi Dt}} \exp\left(-\frac{x^2}{4Dt}\right) \ , \tag{1.2}$$

as can be verified by substitution of this solution into (1.1). The Gaussian nature of the probability distribution $P(x, t)$ was verified through an exchange of ideas and discussions between Pearson and Lord Rayleigh [8, 9].

By multiplying (1.2) with x^2 and integrating over x from $-\infty$ to ∞, we find that the MSD of the BP position increases linearly in time,

$$\left\langle x^2(t) \right\rangle = 2Dt \ . \tag{1.3}$$

The parameter D in (1.1)-(1.3) is known as the diffusion coefficient. Its numerical and analytical determination is the central theme of this thesis.

Although the linear relation (1.3) between the MSD and time was derived from the specific diffusion equation (1.1), it can be obtained from even more general considerations. Namely, the observation time t is divided into a not necessarily large integer number of time intervals Δt with the displacement Δx_n on the n'th interval. The total displacement at time t is given by the sum of individual displacements

$$x(t) = \sum_n \Delta x_n \ . \tag{1.4}$$

The time intervals are chosen to be so large that the displacements are statistically independent:

$$\langle \Delta x_n \, \Delta x_{n'} \rangle = \langle \Delta x^2 \rangle \, \delta_{nn'} \ , \tag{1.5}$$

where $\delta_{nn'}$ is Kronecker delta and $\langle \Delta x^2 \rangle$ is the MSD on an arbitrarily chosen interval. Then, the total MSD becomes

$$\langle x^2(t) \rangle = \sum_{nn'} \langle \Delta x^2 \rangle \, \delta_{nn'} = \sum_{n} \langle \Delta x^2 \rangle = \langle \Delta x^2 \rangle \frac{t}{\Delta t} \ . \tag{1.6}$$

We see that the ratio $\langle x^2(t) \rangle / t = \langle \Delta x^2 \rangle / \Delta t$ is the same for the total observation time t and for each individual time interval Δt. Hence, it must be a constant, as stated by (1.3).

The early investigations of Brownian motion, focused on unraveling the nature of diffusion phenomenon and understanding its underlying mechanisms, laid the foundation for our current understanding of many-body systems. These pioneering studies sparked a profound interest in the dynamics of systems with a few degrees of freedom interacting with a complex environment. Building upon these historical roots, modern research continues to explore and unravel the intricacies of Brownian motion in a wide range of nanoscale entities, such as atoms and molecules [10–12], nanoclusters [13, 14], the scanning probe tip [15–18], proteins in living cells [19], and bacteria [20], to name but a few.

1.2 Langevin and Fokker-Planck equations

Consider Brownian motion of a heavy particle of mass M, momentum $\vec{P}$ and position $\vec{R}$ in a medium consisting of many much lighter atoms of mass m, momenta $\{\vec{p_i}\}$ and positions $\{\vec{r_i}\}$. The total Hamiltonian is

$$H = \frac{\vec{P}^2}{2M} + \sum_i \frac{\vec{p}_i^{\,2}}{2m} + V(\vec{R}, \{\vec{r}_i\}) \ , \tag{1.7}$$

where the first term is the kinetic energy of the heavy atom, the second term is the kinetic energy of the medium, and the third term is the interaction energy of all atoms. Molecular dynamics (MD) simulations [21, 22] require solving the equations of motion

$$\dot{\vec{P}} = -\frac{\partial V}{\partial \vec{R}} \ , \quad \dot{\vec{p}}_i = -\frac{\partial V}{\partial \vec{r}_i} \ , \quad \dot{\vec{R}} = \vec{P}/M \ , \quad \dot{\vec{r}}_i = \vec{p}_i/m \tag{1.8}$$

numerically. This technique is severely limited in terms of the number of the atoms that can be handled and the time scale that can be probed. Fortunately, alternative methods can often be developed that do not have these limitations.

Stochastic modeling is an example of such an alternative. It is possible to replace the full dynamics (1.8) with a reduced version, in which the heat-bath degrees of freedom are integrated out. The generalized Langevin equation (GLE) can be obtained rigorously using the projection operator technique [23], within the harmonic-oscillator heat-bath model [24–29], or with the help of the linear response theory [30]:

$$\dot{\vec{P}} = \vec{F}(\vec{R}) - \int_{-\infty}^{t} ds \overleftrightarrow{\eta}\left(\vec{R}(t), \vec{R}(s), t-s\right)\dot{\vec{R}}(s) + \vec{\xi}\left(\vec{R}(t), t\right) . \tag{1.9}$$

The renormalized force and the noise correspond to the first and last terms of Eq. (1.9), respectively. The second term involves the dissipation kernel denoted by $\overleftrightarrow{\eta}$, is equal to

$$\overleftrightarrow{\eta}\left(\vec{R}(t), \vec{R}(s), t-s\right) = \frac{1}{T}\langle\vec{\xi}\left(\vec{R}(t), t\right)\vec{\xi}^{T}\left(\vec{R}(s), s\right)\rangle . \tag{1.10}$$

This equation is known as fluctuation-dissipation theorem of the second kind [30, 31].

The time-local version of the GLE, known as the standard LE, is introduced by Paul Langevin who was studying Brownian motion [7, 32]. It can be derived from (1.9) if the heat bath dynamics is much faster than the system's. Then, the right-hand side of (1.10) can be approximated by a delta function:

$$\langle\vec{\xi}\left(\vec{R}(t), t\right)\vec{\xi}^{T}\left(\vec{R}(s), s\right)\rangle \approx 2T \overleftrightarrow{\eta}\left(\vec{R}(t)\right)\delta(t-s) . \tag{1.11}$$

The above expression gives the standard LE for the BP

$$\dot{\vec{P}} = \vec{F}(\vec{R}) - \overleftrightarrow{\eta}\left(\vec{R}\right)\dot{\vec{R}} + \vec{\xi}\left(\vec{R}, t\right) . \tag{1.12}$$

1.2.1 Additive and multiplicative noise

In Eq. (1.12), the noise term is additive, meaning it is directly added to the deterministic force term. In this case, the noise correlation function is expressed as

$$\langle \xi(t)\xi(0)\rangle \approx \sigma^2\delta(t) \ , \tag{1.13}$$

where noise strength σ^2 is some constant implying that the noise term in the equation does not depend on the state of the system.

In certain scenarios, noise can exhibit a non-additive impact on system dynamics. In such cases, noise is not just random but also depends on the current state of the system itself, i.e. depends on the particle's velocity, giving rise to what is termed multiplicative noise. It means that the intensity or effect of the noise changes with the particle's velocity. As a result, the LE becomes more complicated and harder to handle [33].

Enter the Stratonovich interpretation, a solution for handling multiplicative noise effectively. This approach incorporates the noise's current and future values (anticipation), thus accounting for the changing intensity of noise's influence on the particle's state. By doing so, the Stratonovich interpretation smoothens out noise's impact. In contrast, the Ito interpretation, deals with noise differently. It considers solely the noise's current value, omitting future times. While this suits certain situations, it falls short in comprehensively addressing the evolving intensity of noise in systems with multiplicative noise and nonlinearity. Consequently, this can lead to distinct predictions and interpretations of particle motion [33].

1.2.2 Gaussian white noise

By the Wiener-Khintchine theorem, noise spectral density is frequency-independent:

$$S(\omega) = \int_{-\infty}^{\infty} dt e^{-i\omega t}\langle \xi(t)\xi(0)\rangle = \sigma^2 \ . \tag{1.14}$$

Due to this property, a delta-correlated noise is called white [34].

In the simulation of a white noise $\xi(t)$ with autocorrelation $\langle \xi(t)\, \xi(t') \rangle = \sigma^2\, \delta(t - t')$, we discretize time, $t \to t_n = n\Delta t$, and produce uncorrelated random numbers, $\xi_n = \xi(t_n)$, at every time step such that $\langle \xi_n \rangle = 0$ and $\langle \xi_n \xi_{n'} \rangle = \frac{\sigma^2}{\Delta t} \delta_{nn'}$. In the limit $\Delta t \to 0$, the autocorrelation function of the noise obtained through numerical methods exhibits a delta-function, $\delta_{nn'}/\Delta t \to \delta(t - t')$, as needed. Generally, the first two moments of a random variable do not provide sufficient information to fully describe its distribution, except when the distribution is Gaussian [35]. It is therefore common practice to estimate the probability density $W(\xi_1, \xi_2, \ldots)$ as

$$W(\{\xi_k\}) = \prod_n W(\xi_n)\ ,\ W(\xi_n) = \frac{1}{\sqrt{2\pi\sigma}} e^{-\xi_n^2/(2\sigma^2)}\ . \tag{1.15}$$

The property of noise being Gaussian can be attributed to the central limit theorem, which holds true when the system interacts with multiple heat-bath atoms simultaneously. Each of these atoms contributes a random force, resulting in a collective random force that is Gaussian in nature [36].

1.2.3 Fokker-Planck equation (FPE)

First, we formulate LE in the most general form. Let the state of the system be characterized by parameters $\underline{z} = (z_1, z_2, ...)$ and let the system be coupled to a heat bath, whose dynamics proceeds much faster than the system's dynamics. Then, the heat-bath effects can be model by the white Gaussian noise processes in the system's equations of motion. Without loss of generality, we can assume them to be mutually independent and have unit strength and zero mean:

$$\langle \xi_i(t) \rangle = 0, \quad \langle \xi_i(t) \xi_j(s) = \delta_{ij} \delta(t - s)\ . \tag{1.16}$$

However, each noise $\xi_j(t)$ is present in the equation of motion of each state variable $z_i(t)$:

$$\dot{z}_i(t) = h_i(\underline{z}) + g_{ij}(\underline{z})\xi_j(t) \tag{1.17}$$

with summation over the repeated index j in the last term implied. The regular force, $h_i(\underline{z})$, and the heat-bath coupling matrix, $g_{ij}(\underline{z})$, are some known functions of the system's state.

At the initial time $t = 0$, the system was in a definite state z_0. We are interested in the system probability density $P(z, t|z_0, 0)$ at a a later time $t > 0$, with the initial condition $P(z, 0|z_0, 0) = \delta(z - z_0)$. The temporal evolution of this transition probability is governed by the Fokker-Planck equations, which is given by

$$\frac{\partial P(\underline{z}, t)}{\partial t} = \frac{\partial}{\partial z_i}\left[\frac{1}{2}\frac{\partial P}{\partial z_k}g_{ij}g_{kj} - \left(h_i - \frac{1}{2}g_{ij}\frac{\partial g_{kj}}{\partial z_k}\right)P\right] . \tag{1.18}$$

Note that the FPE has the form of a continuity equation $\frac{\partial P}{\partial t} = -\vec{\nabla}.\vec{J}$, where the probability current density J consists of three contributions:

1. Diffusive current, $J_{i|diff} = -\frac{1}{2}g_{ij}g_{kj}\frac{\partial P}{\partial z_k}$, which flows from the region with the higher probability to the region with lower probability;

2. Deterministic drift, $J_{i|det} = h_i P$, caused by the deterministic force h_i;

3. The so called Stratonovich drift, $J_{i|Strat} = -\frac{1}{2}g_{ij}\frac{\partial g_{kj}}{\partial z_k}P$, which is zero if the coupling strength to the heat bath $g_{ij}(\underline{z})$, is uniform in the state space of the system. However, if $g_{ij}(\underline{z})$ depends on $\underline{z}$, then the system is coupled to noise in some regions of its state space stronger than in others. Correspondingly, noise will tend to drive the system out of the noisier regions into the less noisy regions, i.e there will be an additional statistical drift [33].

1.3 Stochastic boundary conditions

The most common way to use MD simulations of finite systems is to apply periodic boundary conditions (PBC) in the lateral directions [21,22,37], in which the primary simulation region is surrounded by images of itself. If a particle exits the simulation region at one end, an identical particle reenters the region from the opposite end, i.e. the opposite ends of the simulation box become correlated. These artificial correlations become even worse if the energy released within the simulation region is high compared with the region's average energy. In other words, the MD approach can only be used if the dissipated energy due to some nonequilibrium process under study is relatively small, and thus temperature increase of the simulated region due to this process can be neglected [25].

Attempts to solve these formidable artificial PBC correlations can be classified into four categories. The first category is based on the concept of a heat bath [38, 39]. The second category includes grand canonical molecular dynamics simulations [40, 41]. The third category involves multiscale simulations in which the system is simulated using a combination of MD and a continuum method [42, 43]. The fourth category, which is the focus of Chapter 2, introduces a stochastic boundary region surrounding the simulation volume [24–26].

Stochastic boundary conditions (SBC) are particularly suitable in the simulations of solids. In this method, the object is divided into three regions, namely the simulation region, the boundary region, and the outer region, see Fig. 1.1. The simulation region consists of a central particle and atoms within a certain range from this central particle. Outside the simulation region, the boundary region forms a surrounding shell.

The outermost region is the irrelevant region. In SBC, atoms in the outer region are not simulated explicitly, i.e. the outer region is taken into account in the form of the dissipative and random forces that act on the boundary atoms. The dissipative and random forces

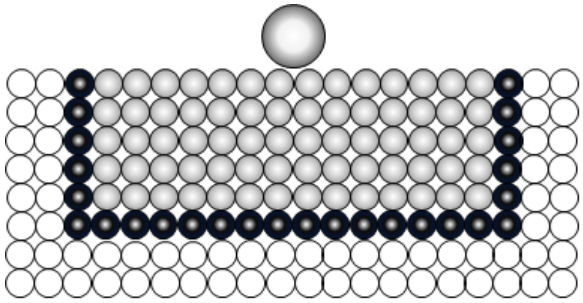

Figure 1.1 – Interaction of a nanosized object, schematically shown as gray bigger circle, with the surface of a solid. The atoms of the solid are divided into the central region (gray circles), the boundary region (black circles), and the outer region (empty circles) that plays the role of a heat bath.

correspond to the interaction between atoms in the central and outer regions. The latter force becomes stochastic due to unknown initial positions and velocities of atoms in the outer region. The balance of these forces helps to maintain the temperature in the central region. The dissipative forces would remove extra energy from the central region, while the random forces perform work on the atoms in the central region whereby bringing energy in. The boundary atoms' equations of motion assume the form of the GLE with colored noise and the damping forces that are not local in time [27, 28]. The damping forces are expressed as time integrals of the boundary atoms' coordinates (or velocities) multiplied by a certain time-dependent dissipation kernel. The noise correlation function is related to the dissipation kernel by the fluctuation dissipation theorem of the second kind [24].

An efficient way to simulate the resulting GLE numerically is to replace the damping and noise terms by a reasonably small number of the fictitious auxiliary degrees of freedom that are coupled to the boundary atoms [29,44,45]. The dynamics of the auxiliary degrees of freedom, in turn, is governed by the regular Langevin equations (LE) with Gaussian white noise and the damping forces proportional to the instantaneous velocities. The parameters of the auxiliary LE are chosen in such a way that the correlation function of the auxiliary

degrees of freedom matches the dissipation kernel in the GLE for the boundary atoms [29, 44, 45].

In such calculations, the highly non-trivial first step is to determine the dissipation kernel in the boundary GLE. This step must involve a few approximations. The first one is treating the solid as harmonic [24–29]. While the harmonic oscillator model allows one to perform an exact derivation of the GLE, the non-linear effects may be significant at elevated temperatures or even at room temperature. The second approximation is that even within the harmonic-solid model, analytic determination of noise and dissipation properties may be too tedious, so that further simplifications, e.g. Debye [28, 29] or Einstein [30] approximation, have to be made. Third, the dissipation and noise terms in the GLE for the boundary atoms are produced not by the bulk, but by the surface atoms of the outer region in contact with the boundary region. What makes things worse, the interface between the boundary and the outer regions is not necessarily planar, see Fig. 1.1 for an example. Hence, the GLE for the boundary atoms is approximate in practice.

Fortunately, the imprecise character of the boundary GLE may not significantly affect the computational accuracy, provided that the boundary region is sufficiently large. Increasing its size makes the surface effects on the boundary region less important. On the other hand, the boundary region should not be too large in order for the simulations to be not too time-consuming. Thus, in every particular problem, a compromise has to be found between computational speed and accuracy.

In chapter 2, an alternative way to impose the SBC is proposed. In this method, the boundary atoms are acted upon by the time-local damping forces and Gaussian white noise that mimics the effect of the environment. That is, no auxiliary degrees of freedom are used. Instead, as originally suggested in [44], the properties of the boundary atoms are renormalized so that their displacement correlation function, as well as displacement

correlation function of atoms in the central region become as similar as possible to that of the atoms of the original solid. Note that the approach introduced here relies not on the full time-dependent correlation function, but on its initial value and its time integral, which can be found either analytically or from numerical simulations of an "infinite" solid with the PBC in all three directions.

Another point of dealing with the MD simulations, a challenging one, is overcoming the limitations with respect to the number of atoms and the time scale that can be handled numerically. In these simulations with the PBC a huge number of the surface degrees of freedom should be simulated explicitly. On the other hand, only a small number of the surface atoms are in immediate contact with the object of interest. Hence, it is intuitively clear that a great deal of computational effort can be saved by simulating only the central region in immediate vicinity of the object, as illustrated in Fig. 1.1. As this object moves on the surface, the central region must move together with it. The method described in Chapter 2 makes such simulations possible.

1.4 Anomalous diffusion

In Section 1.1 we discussed how the diffusion law (1.3) can be obtained by dividing the total observation time into intervals Δt_n large enough for the displacements Δx_n in each to be mutually uncorrelated. This means that the time t in (1.3) must be large.

On the other hand, derivation of the same result from the diffusion equation (1.1) does not rely on this assumption, as the time t in its solution (1.2) can be arbitrarily small. From this, we can conclude that the diffusion equation (1.1) alone does not provide any information about the particle trajectory at small time scales. Indeed, if we observe small displacements, Δx, over a short time interval, Δt, we can determine D by averaging the ratio $\Delta x^2/\Delta t$ as both Δx and Δt approach zero. Since D is finite, $\Delta x/\Delta t$ must be infinite,

which implies that the velocity of a BP, represented as the derivative along a Brownian trajectory curve, is infinite at every point. Consequently, a Brownian trajectory is infinitely jagged, and it is essential to exercise caution when mathematically analyzing Brownian trajectories.

One way to avoid the mathematical complexities of Brownian trajectories is to assume that a random walk motion occurs on a periodic lattice, where jumps take place at regular intervals. In this scenario, the trajectory comprises a connected path of straight line segments. In the long time limit when the number of jumps increases, the random walk solution on a lattice eventually approaches the behavior described by Eqs. (1.1)–(1.3) [1].

There are also situations where Eqs. (1.1)–(1.3) are no longer applicable for the random walks. Fractal time random walks, where the walker waits for long time between jumps, and Lévy flights, where the jumps cover very long distances, are examples. In the case of fractal time random walks, the MSD are slower than in Brownian motion. Conversely, Lévy flights exhibit the characteristic of potentially infinite particle velocities, resulting in extremely long flight lengths. Consequently, the probability distributions associated with particles undergoing Lévy flights may exhibit infinite moments as well. In this case, the emphasis typically lies on the scaling properties of Lévy flights rather than the occurrence of infinite moments. To address the divergence of moments, a velocity is introduced, which is associated with the distance covered during each flight segment. Consequently, instead of considering the MSD of a completed flight, which would be infinite, the focus shifts to the distance traveled by the particle from its starting point up to time t. As a result, Lévy flights exhibit a time-dependent MSD that grows at a faster rate compared to Brownian motion [1, 46, 47].

1.5 Dispersionless transport

The phenomenon of dispersionless transport was originally reported in by Katja Lindenberg et al [48], who simulated the dynamics of a BP in a tilted periodic potential. This phenomenon has gained significant attention in recent years. It is believed that the identification and characterization of dispersionless transport can lead to the development of novel theoretical and computational tools for the analysis and prediction of transport processes in various applications, including material science, chemical engineering, and biophysics [49–53].

The term "dispersionless" suggests that the dispersion, or the MSD, of the BP coordinate should be zero in the dispersionless motion. This means that the trajectory of a BP is deterministic, rather than random, in spite of the thermal noise.

This definition is *not* the one which is adopted in the literature. Rather, dispersionless transport is either defined by a plateau in the particle's coordinate MSD vs. time plot extending over a very broad time interval or by the impossibility to measure the diffusion coefficient within this plateau region. In other words, it is not MSD, but its time derivative which is zero in the dispersionless regime.

In this thesis, we find that both kinds of the dispersionless transport can be observed depending on the model at hand. Namely, in Chapter 2 we find that at the temperature greater than critical temperature, the transport of a BP becomes quasideterministic. After a few acts of interaction with the environment, the BP starts to move at a constant velocity with negligibly small energy dissipation.

In Chapter 3, we examine the dispersionless transport, as defined in [48], more closely for a damped BP in a tilted periodic potential. In contrast to the model studied in Chapter 2, the BP in Chapter 3 and [48] is acted upon by a dissipative force which is proportional to the velocity. We show that the plateau in the particle's position dispersion is, in fact, a

numerical artefact that has to do with the choice of the logarithmic scale on the time axis in the MSD plot. In addition, we show that the impossibility to determine the diffusion coefficient is due to the wild fluctuations of the dispersion which is related to a finite number of stochastic trajectories sampled in a realistic simulation and has nothing to do with the intrinsic properties of the particle dynamics.

Since the MSD is a property of an ensemble of BPs, and its apparently constant value does not necessarily imply that the motion of a single BP from this ensemble is not random. Hence, it is possible to measure the diffusion coefficient also within the dispersionless regime by a modification of the measurement procedure.

1.6 Einstein's relation

The diffusion coefficient D is connected to thermal energy k_BT through the Einstein-Smoluchowski-Sutherland relation

$$D = \frac{k_BT}{6\pi r\eta} , \tag{1.19}$$

where r is the radius of the BP, η is the viscosity of the ambient fluid, and k_B is the Boltzmann constant. By introducing the mobility as $\mu = 1/(6\pi r\eta)$, Eq. (1.19) which is commonly referred to as the Einstein relation can be written as $D = \mu k_BT$. The theoretical foundation of diffusion, especially the relationship between the diffusion coefficient D and thermal energy k_BT initiated a lengthy sequence of experiments focused on enhancing our understanding of diffusive motion. Systematic observations of microscopic diffusing particles introduced protocols for tracking single particle [54]. Time-resolved recordings using a moving film plate avoided the need for ensemble averaging [55] and examining torsional diffusion of a small mirror suspended on a thin quartz thread mapped out of the Gaussian Boltzmann distribution of the equilibrium distribution of angles [56, 57].

It is noteworthy to mention that the Einstein relation is based on the assumption of a

linear relationship between the mean velocity of the BP and the applied force [58]. However, in certain conditions, such as in non-Newtonian fluids or in the presence of strong flow fields or interactions with obstacles, the relationship between the mean velocity and applied force may no longer be linear, leading to a breakdown of the Einstein relation. It has been shown that in supercooled liquids or near phase transitions the temperature dependence of the diffusion coefficient may deviate from the linear relationship [59].

The breakdown of the Einstein relation has been a topic of significant interest in the field of statistical physics. We believe the investigation of the breakdown of the Einstein relation in simple systems can provide valuable insights into the fundamental mechanisms that govern the dynamics of BPs, and can lead to the development of new theoretical models that can better describe the behavior of these particles in complex systems. Therefore, we set our primary objective to investigate the breakdown of the Einstein's relation in simple systems and explore the factors that lead to deviations from this fundamental relationship. In this context, we discuss 1D diffusion of the BP on two different simple models leading to non-Einsteinian relation.

1.7 Organization of the thesis

We reproduce our first paper – diffusion of the BP on the stochastic harmonic oscillator chain (SHOC) model – in Chapter 2. By focusing specifically on the SHOC model, we aim to gain deeper insights into its unique dynamics and explore various physical phenomena within this simplified yet analytically tractable framework. The SHOC model can serve as an ideal testing ground to explore and evaluate alternative approximation schemes intended to replace computationally demanding MD simulations. In order to accomplish this objective, we introduce the concept of the MSBC as an alternative approach in which the SBC is applied to a moving BP. Moreover, we delve into the active research topic of examining

the scaling relation between diffusion and temperature, a crucial aspect that has garnered considerable attention in recent years.

During the investigation of the SHOC model, particularly at high temperatures, two significant phenomena were observed: the "dispersionless" phase and the occurrence of "Lévy flights". The challenge of the dispersionless phase arises when attempting to determine the scaling behavior of the diffusion coefficient with temperature, specifically when the system operates at temperatures surpassing the critical temperature. In this phase, the particle exhibits a constant velocity and minimal energy deposition into the chain. Consequently, the extended interaction time required for the BP to engage with the SHOC surpasses computational limitations, rendering the reliable determination of the diffusion coefficient unattainable. On the other hand, the occurrence of Lévy flights is characterized by the BP demonstrating extensive flight lengths. This phenomenon, commonly referred to as the non-Einsteinian relation, manifests as a non-linear dependence of the diffusion process on temperature. Notably, it was observed that the dissipative force acting on the particle inversely scales with its velocity in this high-temperature regime, which contrasts with the conventional understanding of Brownian motion, where the dissipative force is proportional to velocity in the presence of Gaussian white noise. These intriguing observations motivated us to investigate these two phenomena separately, leading to the development of two distinct models for further exploration.

In pursuit of comprehending the diffusion behavior in the dispersionless phase, Chapter 3 delves into a novel investigation. This chapter presents a reproduction of our second paper, which focuses on the diffusion of BP within a tilted periodic potential. Our findings reveals that this phase is not only characterized by the imposibility to measure the diffusion coefficient but also exhibits a plateau in the particle's coordinate dispersion, persisting over an extended time interval. This plateau phenomenon poses a significant challenge in

accurately measuring the diffusion coefficient within this specific region. In light of these intriguing findings, we embark on an in-depth investigation of dispersionless transport in this chapter, aiming to unravel its underlying principles and shed light on its implications for the behavior of complex systems.

Motivated by the intriguing observation of Lévy flight and its potential implications for diffusion behavior, we embark on an in-depth exploration in Chapter 4. In this chapter, we present a reproduction of our third paper, which focuses on the diffusion of a free BP with velocity-dependent damping. The main objective of this chapter is to investigate the interplay between the inversely proportional dissipative force and velocity at high temperatures, and examine its potential connection to the non-Einsteinian diffusion behavior. Here, through an analytical investigations of the diffusion coefficient, we aim to illuminate fundamental aspects of simple models, diffusion phenomena, and the underlying mechanisms governing the non-Einsteinian relation. By shedding light on these intricacies, our research contributes to advancing our understanding of transport phenomena in complex systems.

In Chapter 5, the thesis presents a comprehensive summary of the findings and contributions of this research. Furthermore, this chapter provides insights into potential future directions and areas of further explorations.

Bibliography

[1] M.F. Shlesinger, J. Klafter and G. Zumofen. Above, below and beyond Brownian motion. *American J. Phys*, **67**, 1253, (1999).

[2] A. Einstein. Über die von der molekularkinetischen Theorie der Wärme geforderte Bewegung von in ruhenden Flüssigkeiten suspendierten Teilchen. *Ann. Phys.*, **17**, 549, (1905).

[3] J. Perrin. *Les Atomes*, 4th ed. (Libairie Alcan, Paris, 1914).

[4] L.S. Ornstein. On the Brownian motion. *Proc. Amst.*, **21**, 96, (1919).

[5] W. Sutherland. A dynamical theory of diffusion for non-electrolytes and the molecular mass of albumin. *Philos. Mag.*, **9**, 781, (1905).

[6] M. Smoluchowski. The kinetic theory of Brownian molecular motion and suspensions. *Ann. Phys.*, **326**, 756, (1906).

[7] P. Langevin. The kinetic theory of Brownian molecular motion and suspensions. *C. R. Acad. Sci.*, Paris, **146**, 530 (1908).

[8] K. Pearson. The problem of the random walk. *Nature*, **72**, 294, (1905).

[9] L. Rayleigh, The dynamical theory of gases and radiation. *Nature*, **72**, 54, (1905).

[10] J.N. Israelachvili. Intermolecular and Surface Forces. *Academic Press, New York*, (1992).

[11] B.N.J. Persson and R. Ryberg. Brownian motion and vibrational phase relaxation at surfaces: CO on Ni(111). *Phys. Rev. B*, **32**, 3586, (1985).

[12] D. Mandelli, W. Ouyang, O. Hod, and M. Urbakh. Negative Friction Coefficients in Superlubric Graphite–Hexagonal Boron Nitride Heterojunctions. *Phys. Rev. Lett.*, **122**, 076102, (2019).

[13] W.D. Luedtke and U. Landman. Slip Diffusion and Lévy Flights of an Adsorbed Gold Nanocluster. *Phys. Rev. Lett.*, **82**, 3835, (1999).

[14] R. Guerra, U. Tartaglino, A. Vanossi, and E. Tossatti. Ballistic nanofriction. *Nature Materials*, **9**, 634–637, (2010).

[15] M.O. Robbins and M.Müser. In Modern Tribology Handbook, edited by B. Bhushan. *CRC Press, Boca Raton*, (2001).

[16] M.R. Sørensen, K.W. Jacobsen and P. Stoltze. Simulations of atomic-scale sliding friction. *Phys. Rev. B*, **53**, 2101, (1996).

[17] M.R. Sørensen, K.W. Jacobsen and H. Jónsson. Thermal Diffusion Processes in Metal-Tip-Surface Interactions: Contact Formation and Adatom Mobility. *Phys. Rev. Lett.*, **77**, 5067, (1996).

[18] P. Reimann and M. Evstigneev. Description of atomic friction as forced Brownian motion. *New J. Phys.* 7, 25, (2005).

[19] C. Di Rienzo, V. Piazza, E. Gratton, F. Beltram, and F. Cardarelli. Probing short-range protein Brownian motion in the cytoplasm of living cells. *Nat. Commun.* 5, 5891, (2014).

[20] G. Li, L.-K. Tam, and J.X. Tang. Amplified effect of Brownian motion in bacterial near-surface swimming. *PNAS* 105, 18355, (2008).

[21] M.P. Allen and D.J. Tildesley. Computer simulation of liquids. *Oxford University Press*, (2017).

[22] D. Frenkel and B. Smit. Understanding molecular simulation: from algorithms to applications. *Elsevier*, **1**, (2001).

[23] H. Mori, H. Fujisaka, and H. Shigematsu. A new expansion of the master equation. *Prog. Theor. Phys.*, **51**, 109, (1974).

[24] L. Kantorovich. Generalized Langevin equation for solids. I. Rigorous derivation and main properties. *Phys. Rev. B*, **78**, 094304, (2008).

[25] L. Kantorovich and N. Rompotis. Generalized Langevin equation for solids. II. Stochastic boundary conditions for nonequilibrium molecular dynamics simulations. *Phys. Rev. B*, **78**, 094305, (2008).

[26] A. Benassi, A. Vanossi , G.E. Santoro and E. Tosatti. Dissipation in sliding friction simulations. *Tribology Letters*, **48(1)**, 41-49, (2012).

[27] V.B. Magalinskii. On the dynamic model in the Brownian theory of motion. *Sov. Phys. JETP*, **9**, 1381, (1959).

[28] R. Zwanzig. Nonlinear generalized Langevin equations. *J. Stat. Phys.*, **9**, 215, (1973).

[29] L. Stella, C.D. Lorenz and L. Kantorovich. Generalized Langevin equation: An efficient approach to nonequilibrium molecular dynamics of open systems. *Phys. Rev. B.*, **89**, 134303, (2014).

[30] M. Evstigneev and P. Reimann. Langevin equation for a system nonlinearly coupled to a heat bath. *Phys. Rev. B.*, **82**, 224303, (2010).

[31] R. Kubo. The fluctuation-dissipation theorem. *Reports on progress in physics*, **29**, 255, (1966).

[32] D.S. Lemons and A. Gythiel. Paul langevin's 1908 paper "on the theory of brownian motion"["sur la théorie du mouvement brownien," cr acad. sci.(paris) 146, 530–533 (1908)]. *American Journal of Physics*, **65**, 1079–1081, (1997).

[33] C.W. Gardiner. Stochastic Methods: A Handbook for the Natural and Social Sciences. Springer Science and Business Media, 2009.

[34] H. Risken. The Fokker-Planck Equation. Springer, 1996.

[35] A. Papoulis, S. Unnikrishna Pillai. Probability, random variables and stochastic processes. (2002).

[36] A.A. Borovkov. Probability theory. *CRC Press*, (1999).

[37] D.C. Rapaport. The art of Molecular Dynamics Simulation. *Cambridge University Press*, (2004).

[38] G. Ciccotti and A. Tenenbaum. Canonical ensemble and nonequilibrium states by molecular dynamics. *Journal of Statistical Physics*, **23**, 767-772, (1980).

[39] A. Tenenbaum, G. Ciccotti and R. Gallico. Stationary nonequilibrium states by molecular dynamics. Fourier's law. *Phys. Rev. A*, **25**, 2778, (1982).

[40] T. Çağin and B.M. Pettitt. Molecular dynamics with a variable number of molecules. *Mol. Phys.*, **72(1)**, 169-175 (1991).

[41] T. Çağin and B.M. Pettitt. Molecular dynamics with a variable number of molecules. *Mol. Sim.*, **6(1-3)**, 5-26, (1991).

[42] SP. Xiao and T. Belytschko. A bridging domain method for coupling continua with molecular dynamics. *Comput. Methods Appl. Mech. Engrg.*, **193**, 1645-1669, (2004).

[43] L.E. Shilkrot, W.A. Curtin and R.E. Miller. A coupled atomistic/continuum model of defects in solids. *Comput. Methods Appl. Mech. Engrg.*, **50**, 2085, (2002).

[44] S.A. Adelman and B.J. Garrison. Generalized Langevin theory for gas/solid processes: Dynamical solid models. *J. Chem. Phys.*, **65**, 3751, (1976).

[45] M. Ceriotti, G. Bussi and M. Parinello. Langevin equation with colored noise for constant-temperature molecular dynamics simulations. *Phys. Rev. Lett.*, **102**, 020601, (2009).

[46] J. Klafter and I.M. Sokolov. First steps in random walks. *Oxford University Press*, Oxford, (2011)

[47] J. Klafter, M.F. Shlesinger and G. Zumofen. Beyond brownian motion. *Physics today*, **49**, 33-39, (1996).

[48] K. Lindenberg, J.M. Sancho, A.M. Lacasta, and I.M. Sokolov. Dispersionless transport in a washboard potential. *Phys. Rev. Lett.*, **98**, 020602, (2007).

[49] W.L. Reenbohn, S. Saikia, R. Roy and M.C. Mahato. Motional dispersions and ratchet effect in inertial systems. *Pramana*, **71**, 297–306, (2008).

[50] S. Saikia and M.C. Mahato. Dispersionless motion in a periodically rocked periodic potential. *Phys. Rev. E*, **80**, 062102, (2009).

[51] S. Saikia and M.C. Mahato. Dispersionless motion and ratchet effect in a square-wave-driven inertial periodic potential system. *J. Phys.: Condens. Matter*, **21**, 175409, (2009).

[52] J.M. Sancho and A.M. Lacasta. The rich phenomenology of Brownian particles in nonlinear potential landscapes. *Eur. Phys. J. Spec. Top.*, **187**, 49–62, (2010).

[53] J. Spiechowicz, P. Hänggi and J. Łuczka. Coexistence of absolute negative mobility and anomalous diffusion. *New J. Phys.*, **21**, 083029, (2019).

[54] J. Perrin. L'agitation moléculaire et le mouvement brownien. *C. R. Acad. Sci.*, **146**, 967, (1908). J. Perrin. Mouvement brownien et réalité moléculaire. *Ann. Chim. Phys.*, **18**, 5, (1909).

[55] I. Nordlund. Eine neue Bestimmung der Avogadroschen Konstante aus der Brownschen Bewegung kleiner, in Wasser suspendierten Quecksilberkügelchen. *Z. Phys. Chem.*, **87**, 40, (1914).

[56] E. Kappler. Versuche zur Messung der Avogadro-Loschmidtschen Zahl aus der Brownschen Bewegung einer Drehwaage. *Annalen der Physik*, **403**, 233, (1931).

[57] R. Metzler. Brownian motion and beyond: first-passage, power spectrum, non-Gaussianity, and anomalous diffusion. *Journal of Statistical Mechanics: Theory and Experiment*, **11**, 114003, (2019).

[58] D. Chandler and J.K. Percus. Introduction to Modern Statistical Mechanics. *Physics Today*, **41**, 114, (1988).

[59] T. Köddermann, R. Ludwig and D. Paschek. On the validity of Stokes-Einstein and Stokes-Einstein-Debye relations in ionic liquids and ionic-liquid mixtures. *Chem. Phys. Chem.* , **9**, 1851-1858, (2008).

Chapter 2

Scaling and universality in the Brownian motion on a stochastic harmonic oscillator chain

In this chapter, we reproduce our first work, authored by Amir Kaffashnia and Mykhaylo Evstigneev, as referenced in [1], with kind permission of the publishers of Physical Review E. The article can be accessed via the DOI: 10.1103/PhysRevE.105.064134.

2.1 Abstract

Diffusion of a Brownian particle along a stochastic harmonic oscillator chain is investigated. In contrast to the usually discussed Brownian motion driven by Gaussian white noise, the particle at high temperatures performs long Lévy flights. At high temperatures T the diffusion coefficient scales as $D \sim T^{2+\alpha}$, where the parameter α determine the average damping force $\propto 1/(T^{\alpha}P)$ on the particle at large momentum P and at high temperature. The exponent α depends on the particle-chain interaction and chain properties. It is shown

that the mean time $\bar{t}_f$ necessary to perform a flight of l lattice constant scales with l as $\bar{t}_f \propto l^{2/3}$ at high temperatures and flight lengths. Last but not least, the flight length probability distribution is found to decay as $1/l^{\beta}$ with the exponent $\beta = 4/3$ being universal, i.e. independent of the model parameters.

2.2 Introduction

Universality is a recurrent theme in physics [2,3]. Simply put, universality means that the scaling exponent α in a relation between two experimental parameters, $y \propto x^{\alpha}$, turns out to be independent of the microscopic details of the system's Hamiltonian. Rather, it is related to a small number of the overall system's properties, such as dimensionality, symmetry, and the interaction range.

Einstein's relation $D/\mu = T$ between the temperature, T, the mobility μ, and the diffusion coefficient, D, of a Brownian particle (BP) is an example of universality with the scaling exponent 1. It typically holds at relatively high temperatures and can be theoretically explained based on an idealized model of a medium consisting of light particles that find themselves in a close-to-equilibrium state weakly perturbed by the BP. This idealized picture does not always apply to real systems, and therefore the breakdown of Einstein's relation became an active research topic recently [4–13].

The simplest model where the breakdown of the Einsteinian diffusion scaling can be expected is a one-dimensional harmonic oscillator chain. Due to its rationality and integrability, this model has inspired theoretical interest since the original treatment by Schrödinger [14]. Its usefulness in the field of statistical physics lies in the fact that it can serve as a heat bath model [15, 16]. In recent years, this model has been extended and widely applied to a variety of phenomena, such as particle [17, 18] and energy diffusion [19,20], atom/solid scattering [21], heat conduction [22], and stochastic resonance [23].

It has also been considered in the context of polaron physics [24, 25] and nanoscale friction [26,27]. Last but not least, diffusion of a BP along a harmonic oscillator chain may serve as a minimal description of transport of atoms and molecules through a one-dimensional channel, such as a carbon nanotube [28, 29].

About 15 years ago, Silvius, Parris, and De Bièvre studied the diffusion of a BP along a chain of independent harmonic oscillators with piecewise-constant interaction potential between a representative oscillator and the BP. The authors reported a non-Einsteinian asymptotic behavior of the diffusion coefficient with temperature, namely, $D \propto T^{5/2}$ at high temperatures [24].

This observation brings up some intriguing questions. First, can the same 5/2 scaling be observed in other models of one-dimensional diffusion, which are more general than the one from [24]? Are other values of the diffusion scaling exponent possible? Are those values universal, i.e. do they apply to a broad range of system's properties and depend only on the system's features, such as dimensionality and interaction range? Can universal scaling relations be expected between other parameters that characterize the one-dimensional diffusion process? Are the exponents appearing in different scaling relations related to each other?

In this paper, we study the diffusion of a Brownian particle along a stochastic harmonic oscillator chain (SHOC), introduced originally in the paper [18]. The system studied here and in [18] differs from the model of Silvius et al [24] in several respects. First, in contrast to [24], the oscillators in our SHOC are not independent. Second, in the present work, the particle-oscillator potential is a smooth function of distance between these objects. Third, the SHOC oscillators find themselves in contact with a Langevin heat bath, whereas the oscillators in the model [24] perform noise-free harmonic motion with the random initial coordinates and velocities chosen from the Maxwell-Boltzmann distribution. As a result

of these differences, we find a different scaling of the diffusion coefficient with temperature than $D \propto T^{5/2}$ in [24].

The main qualitative difference between the BP/SHOC diffusion discussed here and in [18,24] from the standard Brownian motion is that the BP in our case moves predominantly via long flights at high T. This kind of motion has been reported earlier in the molecular dynamics studies of adatom diffusion on solid surfaces [30–32]. The physical reason for long flights is that the chain oscillators (or the atoms of the substrate in [30–32]) do not absorb the energy from the rapidly moving BP as from a slow BP. In contrast, in the standard Brownian motion with $D \propto T$, the BP always experiences a damping force, which linearly increases with its velocity.

As stated earlier, our BP/SHOC model was introduced in [18]. The main goal of that paper was to work out a simplified Langevin description of the BP dynamics and to investigate the limitations of this description. Here, we focus on the scaling relations that characterize the BP/SHOC system, especially the relation between the diffusion coefficient and temperature and the scaling of the BP flight length distribution. To achieve this task, we develop a numerical procedure to simulate the BP trajectory more efficiently than the method employed in [18]. As a result of extensive simulations we establish that the diffusion coefficient in this model scales with temperature as $D \propto T^{2+\alpha}$ with the parameter $\alpha \geq 0$ that depends on the system properties. The scaling is shown to stem from the dependence of the mean friction force on the particle momentum and temperature. While the exponent $2 + \alpha$ is not universal, two universal scaling relations are found in the BP/SHOC system. Namely, the mean flight time, $\bar{t}_f$, scales with the flight length, l, as $\bar{t}_f \propto l^{2/3}$, independent of the system parameters. Second, the flight length probability distribution is found to decrease as $w_l \propto 1/l^{4/3}$ in a broad interval of flight lengths l. Eventually it exponentially drops to zero at large l, so that the moments of this distribution remain finite.

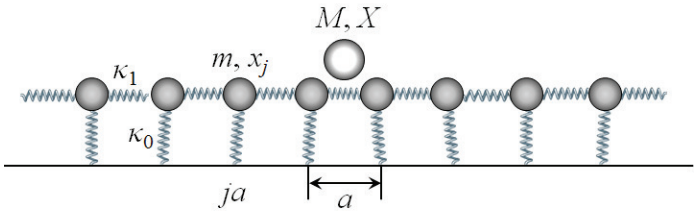

Figure 2.1 – The BP/SHOC model discussed in this paper, with the BP schematically shown as a circle on top of the chain oscillators.

This paper is organized as follows. In the next section, the SHOC model [18] is briefly described. Then, the results of the diffusion coefficient measurements are presented in Section 2.4. In order to explain those results, a simple theory is worked out in Section 2.5 and its predictions are tested in Section 2.6. The flight length probability distribution is presented and discussed in Section 2.7, after which the main findings of this paper are summarized. The simulation details are explained in Appendix 2.A and the methodology used to extract the diffusion coefficient from the numerical data is described in Appendix 2.B.

2.3 The model

We consider the one-dimensional motion of a BP of mass M and position X along an infinite periodic chain of stochastic harmonic oscillators of mass m and positions x_j, as described in [18], see Fig. 2.1. The equation of motion of the BP reads

$$M\ddot{X} = -\sum_j W'(X - x_j) \ , \tag{2.1}$$

where $W(X - x_j)$ is the interaction potential between the BP and the jth oscillator of the chain. For definiteness, a Gaussian potential

$$W(x) = -\varepsilon\, e^{-x^2/(2\sigma^2)} \tag{2.2}$$

of depth $\varepsilon > 0$ and width σ is assumed, as in the earlier work [18]. This potential is short-ranged, attractive, smooth, and goes to zero at large distances, making the BP diffusion along the chain possible.

The mechanical equilibrium positions of the chain oscillators are regularly spaced with periodicity a. Hence, the coordinate of a jth oscillator can be decomposed into

$$x_j = ja + u_j \ , \tag{2.3}$$

where u_j is the displacement from mechanical equilibrium. The chain oscillators are assumed to be pinned to the lattice sites at ja by springs of stiffness κ_0 and connected to the nearest neighbors by springs of stiffness κ_1 and rest length a. It is furthermore assumed that each oscillator is coupled to its own heat bath, modeled by the dissipative and random forces. The chain equations of motion read:

$$\begin{aligned} m\ddot{u}_j = &-\kappa_0 u_j - \kappa_1(2u_j - u_{j-1} - u_{j+1}) \\ &+W'(X - ja - u_j) - \gamma\dot{u}_j + \sqrt{2\gamma T}\xi_j(t) \ . \end{aligned} \tag{2.4}$$

Here, T is the thermal energy, γ is the damping coefficient, and Gaussian white noises $\xi_j(t)$ are such that

$$\langle \xi_j(t) \rangle = 0, \quad \langle \xi_j(t)\xi_{j'}(t') \rangle = \delta_{jj'}\delta(t - t') \ . \tag{2.5}$$

In the simulations reported below, four sets of parameter values were tested with

$$\kappa_0 = 1 \, , \quad \gamma = 0.1 \, , \ a = 1 \, , \quad m = 1 \, , \quad M = 10 \, , \ \sigma = 0.2 \ . \tag{2.6}$$

The four parameter sets differed in the values of κ_1, which was either 1 or 0 (interacting vs. non-interacting oscillators), and ε, which was either 0.1 or 1 (weak vs. strong particle-chain coupling). In addition, we performed simulations for other parameter values, namely, increasing and decreasing the BP mass M and the interaction energy ε by an order of magnitude relative to the respective values from (2.6). The scaling exponents that are termed 'universal' in this paper had the same values for all parameters tested.

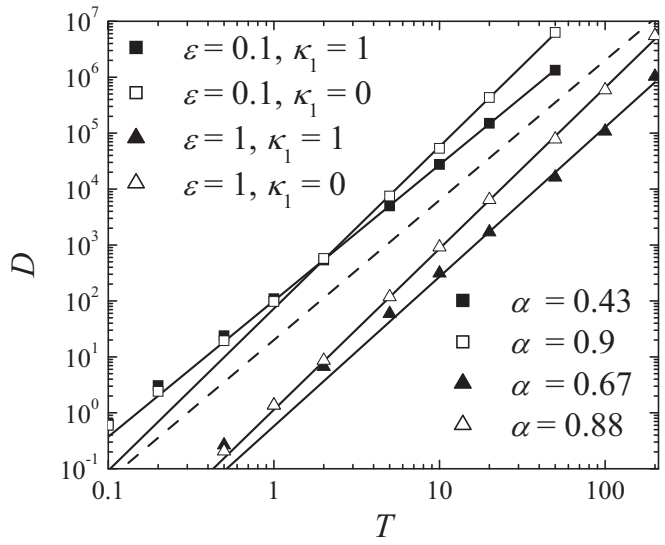

Figure 2.2 – Temperature dependence of the diffusion coefficient for the 4 parameter sets tested, as obtained from the simulations (symbols), and the fit of the simulation data at five largest temperatures with the power law formula (2.9) (solid lines). The scaling exponent α for each data set is indicated in the legend. For reference, the curve $D \propto T^{2.5}$ is shown as the dashed line.

2.4 Diffusion coefficient scaling

2.4.1 Temperature dependence of the diffusion coefficient

The random motion of the BP is characterized by the time-dependent diffusion coefficient, defined as

$$D_t = \frac{\langle \Delta X^2(t) \rangle}{2t} \ , \quad \Delta X(t) = X(t) - X(0) \ . \tag{2.7}$$

As a function of time, D_t initially increases in the ballistic regime, and eventually enters the diffusive regime, where it saturates at the long-time value

$$D = \lim_{t \to \infty} D_t \ , \tag{2.8}$$

which is of our main interest.

A straightforward way to find D is to simulate the stochastic trajectory $X(t)$ over a long observation time t_{obs} and then to average over many such trajectories. This approach is rather time-consuming, because the transition from the ballistic to the diffusive regime may be quite long [18]. Therefore, we used a different method, which is faster and more efficient. The general idea of this procedure is to take advantage of the fact that the BP trajectory consists of flights over at least one lattice constant separated by the rest phases, during which the BP remains bound to one of the SHOC oscillators. Then, a reasonably small flight phases are grouped into segments, such that the displacement S_k in the kth segment is statistically independent of the displacement S_{k-1} in the previous segment. The diffusion coefficient is then calculated as $D = \sum_k \langle S_k^2 \rangle / (2t_{obs})$, where t_{obs} is the time over which the particle trajectory is observed. The details of the numerical algorithm to evaluate D from the simulation data are given in the Appendix 2.B.

Figure 2.2 shows the diffusion coefficient vs. temperature plots for the four parameter sets from Eq. (2.6) and below. At the temperatures below $T = 5$, the diffusion coefficient does not seem to depend on the chain interaction stiffness κ_1, as the two weak-coupling curves (open and closed squares above the dashed line) and the two strong-coupling ones (open and closed triangles below the dashed line) seem to converge. At high temperatures, on the other hand, all four curves can be fitted by a power law

$$D(T) = KT^{2+\alpha} \tag{2.9}$$

with different values of the exponent α indicated in the legend of Fig. 2.2. The solid straight lines in Fig. 2.2 are the fits of the diffusion coefficient at the five highest temperatures probed (weak-coupling case: $T = 2$, 5, 10, 20, and 50; strong-coupling case: $T = 10$, 20, 50, 100, and 200). The scaling exponent α obtained from the fitting are close, but not quite identical to the value 0.5 reported in [24] with the largest deviation observed for the parameter sets with $\kappa_1 = 0$, for which $\alpha \approx 0.9$. This discrepancy in α stems from the difference in the

models studied in [24] and here, see Section 2.2.

At this point, we can make a preliminary conjecture that the exponent α in Eq. (2.9) is not universal. It depends on the SHOC properties and on the particle-chain interaction potential. But the following reservations need to be borne in mind.

First, the choice of the five largest temperatures for the linear fit may seem arbitrary, as all data points do not deviate much from the straight line on the double logarithmic scale in Fig. 2.2; this means that the α-values obtained are not necessarily accurate.

On the other hand, it is not obvious that those five highest temperatures are high enough to establish the truly asymptotic value of the exponent α. It is possible that at $T > T_{max}$ (with $T_{max} = 50$ for the weak-coupling and $T_{max} = 200$ for the strong-coupling case) the curves would be described by a different exponent α, which may (or may not) turn out to be the same for all four parameter sets.

Unfortunately, going to higher temperatures turns out to be difficult, because increasing the temperature above T_{max} results in an increase of the typical flight length, whose distribution will be discussed in the last section of this paper. As a matter of fact, at $T = 2T_{max}$, flights can become so long that the BP does not come to rest after several hours of simulations.

2.5 Flight length and flight time scaling

2.5.1 Time of flight and flight length

To better understand the origin of the scaling (2.9) and to find out, which temperature is high enough to be deemed asymptotically large, answer this question, we need to find an alternative way to measure the exponent α. For this purpose, we adopt and generalize the argument from [24] (especially Section II of this work) to establish various scaling laws that

will be used later to discuss the simulation data in greater detail.

The force $-\sum_j W'(X - x_j)$ acting on the BP in (2.1) is a random function of time due to the thermal motion of the SHOC oscillators. After averaging with respect to the SHOC fluctuations, it should become a periodic function of X with the lattice periodicity a. Furthermore, after averaging with respect to a lattice period, it should become a function of the BP velocity only, because the response of the SHOC coordinates x_j to the BP motion depends on how fast the BP moves.

Since we are interested in the diffusion coefficient at high temperatures, we consider the case of a high initial velocity right in the beginning of a flight phase. A fast BP generates the potential $W(X_t - x)$ that changes in time so quickly that the oscillators cannot follow its temporal variations due to their own finite reaction time. Hence, the faster the BP moves, the slower the rate at which it deposits energy into the chain.

Consider the coarse-grained momentum of the BP

$$P(t) := M\frac{X(t+\tau/2) - X(t-\tau/2)}{\tau} \ . \tag{2.10}$$

The coarse-graining time τ must be much larger than the time necessary to cover one lattice period, but much shorter than the overall time of flight. Due to this averaging, the stochastic and periodic aspects of the force in the equation for P can be neglected. The average force is purely dissipative. We expect that at large P it is inversely proportional to some power of the coarse-grained momentum:

$$\frac{dP}{dt} = -\frac{A_\mu}{P^\mu} \tag{2.11}$$

with some constant $A_\mu > 0$ and $\mu > 0$. This equation, with the exponent $\mu = 2$, was originally derived in [24] (see Eq. (2.17) of that work). We will treat the exponent μ and the coefficient A_μ as parameters to be found from a numerical experiment. The time differential $dt \sim \tau$ in (2.11) should be understood in the coarse-grained sense, as explained

above.

In order for the friction force to be opposite to the BP direction of motion, Eq. (2.11) would have to be formulated more generally as $dP/dt = -A_\mu P/|P|^{\mu+1}$. But to keep the notation slightly simpler, we assume that $P > 0$. For brevity, we will omit the words "coarse-grained" and refer to P simply as momentum in the rest of the paper.

A flight phase consists of two stages. Initially, the particle moves so fast that it deposits very little energy into the chain and, in turn, the random motion of the chain oscillators has very little effect on the BP. It is in this first stage, described by (2.11), that the BP covers most of the distance. Eventually, the second stage begins, in which equation (2.11) is no longer accurate. The interaction between the BP and the chain becomes stronger, leading to a fast energy transfer from the BP to the chain and in a more pronounced randomization of the BP trajectory by the stochastic oscillators. In this second stage, the BP quickly slows down and eventually gets trapped by one of the chain oscillators.

In the first stage, the momentum decrease per unit length is

$$\frac{dP}{dX} = \frac{dP}{dt}\frac{dt}{dX} = -\frac{MA_\mu}{P^{\mu+1}} \ . \tag{2.12}$$

Integrating this from the initial momentum P to zero gives the flight length as a function of the initial momentum:

$$L(P) = -\int_P^0 dP' \, \frac{P'^{\mu+1}}{MA_\mu} = \frac{P^{\mu+2}}{(\mu+2)MA_\mu} \ . \tag{2.13}$$

Likewise, integrating equation (2.11) gives the time of flight as a function of the initial momentum:

$$t_f(P) = \frac{P^{\mu+1}}{(\mu+1)A_\mu} \ . \tag{2.14}$$

Eqs. (2.13) and (2.14) in the special case $\mu = 2$ are also obtained in [24]. The actual length and duration of each flight may differ from the expressions (2.13) and (2.14) due to the randomizing effect of the chain in the second stage of the flight, which is neglected in

(2.11). Those random deviations from (2.13) and (2.14) need to be small in order for the assumptions behind Eq. (2.11) to be valid.

2.5.2 Temperature dependence of the diffusion coefficient

In view of the definition (2.10) there is no a priori reason to assume that the probability distribution $\rho(P)$ of the initial momentum P is Maxwellian, as done in [24]. In addition to temperature, it may depend on the properties of the SHOC, as well as on the oscillator-particle interaction potential. But we can expect that at high temperatures those additional parameters should become relatively unimportant as compared to the thermal energy. Because dimensional consistency requires that the argument of any non-linear function be non-dimensional, the initial momentum probability distribution at high temperatures is expected to be of the form

$$\rho(P) = f(P/\sqrt{MT})/\sqrt{MT} \ , \tag{2.15}$$

where the function $f(x)$ is even and normalized to one: $f(-x) = f(x)$, $\int_{-\infty}^{\infty} dx\, f(x) = 1$. The factor $\sqrt{MT}$ in (2.15) is necessary for the correct normalization of $\rho(P)$.

Based on this information, we can use Eqs. (2.13) and (2.14) to find the scaling of the mean flight length squared, $\langle L^2 \rangle = \int dP\, L^2(P)\, \rho(P)$, and the mean flight time, $\langle t_f \rangle = \int dP\, t_f(|P|)\, \rho(P)$, with temperature:

$$\begin{aligned} \langle L^2 \rangle &= \frac{M^\mu T^{\mu+2}}{[(\mu+2)A_\mu]^2} F_{2(\mu+2)} \ , \\ \langle t_f \rangle &= \frac{(MT)^{(\mu+1)/2}}{(\mu+1)A_\mu} F_{\mu+1} \ , \\ F_n &:= \int dx\, |x|^n\, f(x) \ . \end{aligned} \tag{2.16}$$

As for the mean rest time, it decreases with temperature and is much smaller than the flight time, $\langle t_r \rangle \ll \langle t_f \rangle$ (see Eq. (2.49)), as was confirmed by the simulations. Therefore,

the diffusion coefficient at high temperatures is given by

$$D = \frac{\langle L^2 \rangle}{2 \langle t_f \rangle} = \frac{F_{2(\mu+2)}}{F_{\mu+1}} \frac{\mu+1}{2(\mu+2)^2} M^{(\mu-1)/2} \frac{T^{(\mu+3)/2}}{A_\mu} \ . \tag{2.17}$$

This expression is approximate, as it neglects the correlations between the consecutive flight lengths. However, as we verified numerically, their contribution does not exceed 5 %, see inset in Fig. 2.7(b), where (2.17) corresponds to the D-value with $\nu_{min} = 1$.

Now we can make a reasonable guess about the origin of the exponent α. There is no a priori reason to assume that the parameter A_μ should be a temperature-independent constant, even though this turned out to be the case in [24]. The higher the temperature, the less sensitive should the chain dynamics be to the fast BP motion, and so the less energy should the chain absorb from the BP. Hence, we can expect that A_μ should decrease with T. Assuming a power-law relation

$$A_\mu(T) = \frac{B_\mu}{T^\alpha} \tag{2.18}$$

with $B_\mu = \text{const}$, the diffusion coefficient should scale with temperature as $D \propto T^{\alpha+(\mu+3)/2}$. For $\mu = 1$, Eqs. (2.17) and (2.18) give $D \propto T^{2+\alpha}$, Eq. (2.9).

2.5.3 Determination of the scaling exponents α and μ

The simplified model (2.11) contains two parameters: the scaling exponent μ and the coefficient A_μ. Both can be estimated based on the expressions (2.13) and (2.14). Indeed, the initial momentum P can be expressed in terms of the flight length L using (2.13), and substitution of the result into (2.14) gives the duration of a flight expressed in terms of its length:

$$t_f(L) = \frac{[(\mu+2)M]^{(\mu+1)/(\mu+2)}}{(\mu+1)A_\mu^{1/(\mu+2)}} L^{(\mu+1)/(\mu+2)} \ . \tag{2.19}$$

It then follows that a log-log plot

$$\ln(t_f(L)) = \ln(t_0) + \frac{\mu+1}{\mu+2}\ln(L/a)\ ,$$
$$t_0 = \frac{[(\mu+2)aM]^{(\mu+1)/(\mu+2)}}{(\mu+1)A_\mu^{1/(\mu+2)}} \tag{2.20}$$

should be a straight line, whose slope, $\frac{\mu+1}{\mu+2}$, can be used to find the exponent μ; after μ is found, one should be able to determine the constant A_μ from the intercept of this line with the y-axis, i.e. from the parameter t_0. A deviation of the $\ln t_f$ vs. $\ln L$ plot from a straight line would immediately signal the inadequacy of Eq. (2.11) to describe the long flights of the BP.

2.6 Results and discussion

2.6.1 Flight time, flight length, and diffusion coefficient

Figure 2.3(a) shows the natural logarithm of flight time vs. flight length for each flight observed in the simulations at $\kappa_1 = 1$, $\varepsilon = 0.1$ and $T = 1$ (gray circles). The solid black line in this figure is the mean flight duration $\bar{t}_f$ averaged over all flights that have the same length $|l|$, where l is defined by Eq. (2.46). It is clear that at the flight length exceeding several lattice constants, both data sets can be fitted with a straight line, as predicted by (2.20). All other parameter sets tested yielded very similar plots of $\ln t_f$ vs. $\ln L$ at $T > 0.1$. At lower temperatures, long flights were absent, and the particle motion proceeded via hopping by just one lattice constant.

Shown in Fig. 2.3(b) is the average time of flight vs. flight length obtained from the simulations (gray curves) and the straight-line fits to the simulation data (black lines). On the double logarithmic scale, the simulation curves obtained at $T \geq 0.5$ have practically the same slope of 0.67, with variations not exceeding 5 % of this value. As for the lowest temperature $T = 0.1$, the $\ln \bar{t}_f$ vs. $\ln |l|$ curve likewise can be fitted with a straight line with

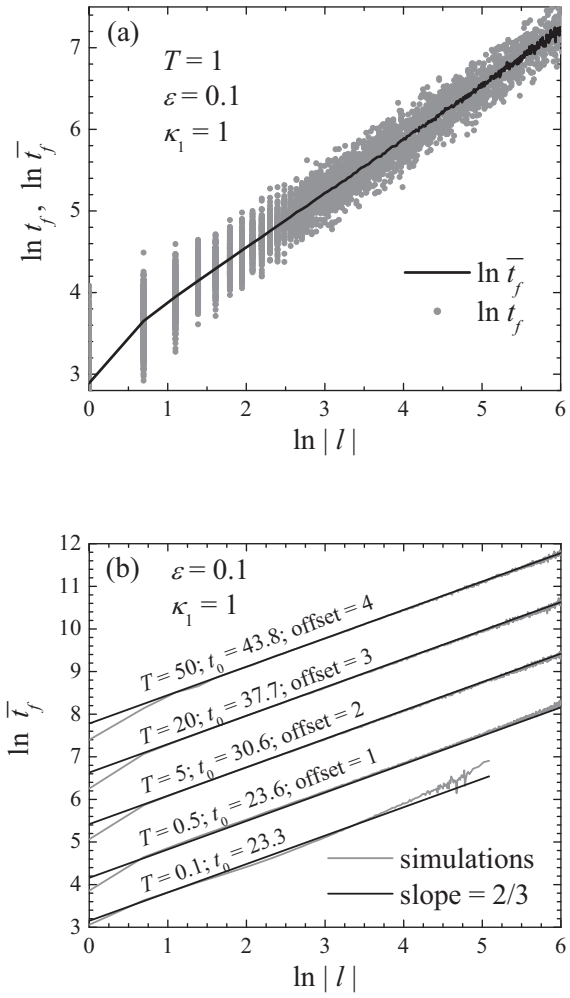

Figure 2.3 – (a) Symbols: the raw simulation data showing the time of flight t_f vs. flight length expressed as an integer multiple of the lattice constant, see Eq. (2.46). Solid line: the average time of flight $\bar{t}_f$ vs. flight length $|l|$. (b) Average time of flight vs. flight length (gray curves) obtained for several temperatures from $T = 0.1$ to 50 together with linear fit with (2.20) (black lines). To avoid overlapping, the curves are shifted vertically with respect to the one at $T = 0.1$. The values of the temperature, the parameter t_0 from (2.20), and the offset are shown at each curve.

the slope of 0.67 reasonably well, see the lowest curve in Fig. 2.3(b). However, the best straight-line fit has the slope value of 0.78. At a slightly higher temperature $T = 0.2$ (not

shown in Fig. 2.3(b)), the best-fit slope turned out to be 0.74.

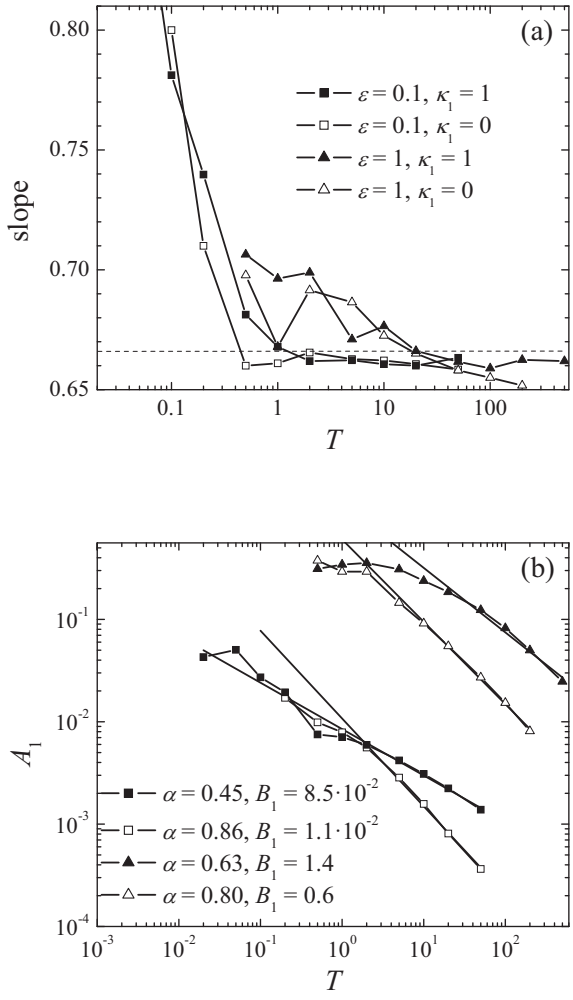

Figure 2.4 – (a) The slope of the straight-line fits to the $\ln \bar{t}_f$ vs. $\ln |l|$ curves as a function of temperature for all four parameter sets tested, as indicated in the legend. (b) The parameter A_1, obtained from the intercept of the $\ln \bar{t}_f$ vs. $\ln |l|$ straight-line fits with the y-axis. In the fitting procedure, the slope of all straight lines was assumed to be 2/3 regardless of temperature. The fit was performed for $|l| \geq 10$, i.e. only flights of length exceeding 10 lattice constants were regarded as long. The legend shows the values of the fit parameters α and B_1 from (2.18), as obtained from this fit for each parameter set.

The slope of the $\ln \bar{t}_f$ vs. $\ln |l|$ curves as a function of temperature for all four parameter sets tested is shown in Fig. 2.4(a). It is seen that it increases on cooling. But at high temperatures $T > 5$, it converges for all parameter sets to the value of $2/3$, shown in Fig. 2.4(a) as a dashed horizontal line. Small deviations from this value do not exceed 5 % and can be attributed to statistical uncertainty. This implies that the exponent in (2.20) equals

$$\mu = 1 \ , \tag{2.21}$$

as conjectured in the end of Section 2.5.2. This value is perhaps unsurprising in view of the fact that the mean friction force at large momenta should be an analytic function of $1/P$, whose leading-order term is written in the right-hand side of (2.11). Because the typical BP momentum increases with T as $\sqrt{MT}$, the higher powers of $1/P$ should be more important at low than at high temperatures, which explains the deviation of the slope from the value 0.67 observed on cooling.

The temperature variations of the intercept in (2.20), $\ln(t_0)$, can be attributed to the temperature dependence of the parameter A_1 in (2.11). The coefficient A_1 can be extracted from the second equation (2.20) (with $\mu = 1$) as

$$A_1 = \frac{9}{8} \frac{(aM)^2}{t_0^3} \ . \tag{2.22}$$

The variations of A_1 with T for all four parameter sets are shown in Fig. 2.4(b). To produce this plot, the parameter t_0 is obtained by fitting $\ln \bar{t}_f$ vs. $\ln |l|$ with a straight line with the slope set to the value $2/3$ regardless of the temperature, i.e. only $\ln t_0$ was a fit parameter. It is to be borne in mind that this procedure is not quite correct at low temperatures, i.e. the so obtained A_1-values at low temperatures are unreliable. Fortunately, Fig. 2.4(a) gives us the temperature range at which the slope is close to the value $2/3$, and thus the numerical values of A_1 so obtained are trustworthy.

It is seen that for each data set, the last five data points can be accurately fitted with a straight line on the double logarithmic scale according to equation (2.18). The slope of those fits is just the exponent α, whose values are shown in the legend of Fig. 2.4(b).

It is remarkable that they agree with the values obtained from the measurements of the diffusion coefficient to within 10 %, cf. Fig. 2.2. This agreement signals the essential correctness of the simplified treatment of Section 2.5. It also suggests that the exponent α depends on the particle-chain interaction parameters and therefore is not universal, as suggested earlier.

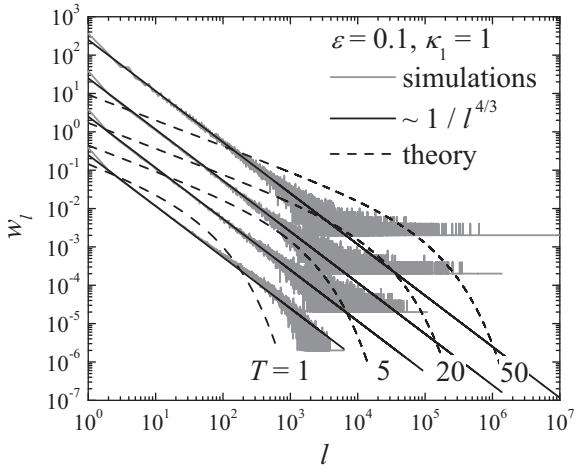

Figure 2.5 – Flight length probability distribution w_l for $\varepsilon = 0.1$ and $\kappa_1 = 1$ at 4 temperatures, $T = 1$, 5, 20, and 50, as obtained from the simulations (gray curves). To avoid curve overlapping, the probabilities w_l at $T = 5$, 20, and 50are multiplied by 10, 100, and 1000, respectively. Black lines are $\propto 1/l^{4/3}$. Dashed lines are obtained with Eq. (2.28).

2.7 Flight length probability distribution

Finally, it is instructive to consider the distribution w_l of flight length measured in units of the lattice constant. In view of the definition (2.46), it is given by

$$w_l = \int_{P_l}^{P_{l+1}} dP\, \rho(P) \ , \tag{2.23}$$

where $P_l = (3aMA_1 l)^{1/3}$ is the initial momentum that results in a flight length of l lattice constants, as follows from (2.13) with $L = la$ and $\mu = 1$. For large $l \gg 1$, the difference between the initial and the final momenta is small,

$$P_{l+1} - P_l \approx \frac{(aMA_1)^{1/3}}{(3l)^{2/3}} \ , \tag{2.24}$$

as can be obtained by expanding P_{l+1} in $1/l$ to the first order. Hence, the probability w_l can be approximated as

$$w_l = \rho(P_l)(P_{l+1} - P_l) \propto \frac{f(P_l/\sqrt{MT})}{l^{2/3}} = \frac{f((l/\lambda)^{1/3})}{l^{2/3}} \ , \tag{2.25}$$

where we combined Eqs. (2.15) and (2.24) and introduced the characteristic length

$$\lambda = \frac{\sqrt{M}T^{3/2}}{3aA_1} = \frac{\sqrt{M}}{3aB_1} T^{\alpha+\frac{3}{2}} \ . \tag{2.26}$$

As stated earlier, since P is the coarse-grained rather than kinematic momentum, the distribution of P is not necessarily Maxwellian. Nevertheless, it can be reasonably expected that at large momenta, the effect of the SHOC fluctuations on the BP state of motion diminishes, and so the difference between the coarse-grained and kinematic momentum should also decrease with P. Hence, at high momenta, its probability distribution should behave as

$$\rho(P) \propto e^{-P^2/(2MT)} \ , \tag{2.27}$$

i.e. $f(x) = (2\pi)^{-1/2}\, e^{-x^2/2}$, see Eq. (2.15). This implies that at large l, we should have

$$w_l \propto \frac{e^{-(l/\lambda)^{2/3}/2}}{l^{2/3}} \ . \tag{2.28}$$

Shown in Fig. 2.5 are the probability w_l vs. l curves for $\varepsilon = 0.1$ and $\kappa_1 = 1$, as obtained for the temperatures $T = 1$, 5, 20, and 50 from the simulations (gray lines) and from the asymptotic formula (2.28) (dashed lines). As can be seen in Fig. 2.5, the agreement between the simulation and the expected curve (2.28) is only qualitative. Both sets of data are described by an initial linear decrease of $\ln w_l$ vs. $\ln l$ followed by an exponential drop of w_l to zero. But this is as far as their similarity goes.

The most striking feature of the simulation curves is that initially, they all exhibit the same power-law decay according to

$$w_l \propto l^{-\beta} \tag{2.29}$$

with the exponent β conspicuously close to the value 4/3, as opposed to 2/3 predicted by (2.28). In fact, we observed the same $1/l^{4/3}$ decay of w_l for all 4 parameter sets tested at temperatures $T > 1$. Therefore, we believe that the value $\beta = 4/3$ is indeed universal. Unfortunately, we cannot offer its satisfactory explanation.

2.8 Conclusions

We have considered the diffusion of a Brownian particle (BP) along a stochastic harmonic oscillator chain (SHOC). An efficient algorithm to simulate this process numerically is developed. Its main idea is to simulate explicitly only a reasonably small section of the chain and to account the rest of the chain by renormalizing the properties of the first and the last oscillators of this segment. As the particle moves, the chain segment moves together with it so that the particle always finds itself in its middle. Although this method proved to be successful in the one-dimensional simulations performed in this paper, we expect that it can be applied, with suitable modifications, to study the two-dimensional diffusion of atoms on solid surfaces.

A method to find the particle's diffusion coefficient from the simulations data is de-

veloped. It makes optimal use of the flight lengths and times, as well as the rest times generated in the simulations. Application of this method to the BP/SHOC diffusion revealed that the diffusion coefficient scales with temperature as $D \propto T^{2+\alpha}$ at asymptotically high temperatures with the non-universal exponent α that depends on the particle-chain interaction parameters and on the chain properties.

A way to identify this asymptotically high temperature regime is proposed. It is based on measuring the average flight time $\bar{t}_f$ necessary for the BP to perform a flight of a given length l. In the temperature range where the $D \propto T^{2+\alpha}$ scaling is valid, the expected relation between these two quantities is $\bar{t}_f \propto l^{2/3}$ independent of the system parameters, as confirmed in the simulations. This method also offers an alternative way to measure the diffusion scaling exponent α, which turned out to be in good agreement with the results of the D vs. T measurements.

Finally, the flight length probability distribution w_l is shown to decay as $w_l \propto 1/l^{\beta}$ with a universal exponent β independent of the system parameters. The value $\beta = 4/3$ found in the simulations awaits its theoretical interpretation.

The obvious discrepancy between the simulation results and the expected probability distribution (2.28) indicates that although the theory adopted here does explain some aspects of the BP/SHOC dynamics, it is incomplete. We conjecture that it can be improved in two principal directions.

First, the distribution of the initial momentum probably differs from the Maxwellian formula (2.27), at least at small P. In fact, replacing the (2.27) with $\rho(P) \propto e^{-P^2/(2MT)}/P^2$ translates nicely into $w_l \propto 1/l^{4/3}$. However, a physical motivation for such a replacement (other than fitting the w_l curve) is unclear. Finding the correct form of the initial momentum distribution should be performed in the future.

The second improvement is to include the possibility of momentum fluctuations during

the long flight, i.e. to replace the coarse-grained equation of motion (2.11) with some sort of a Langevin-like description for the actual kinematic momentum. A replacement of the full dynamics (2.1)-(2.4) with a Langevin equation for the BP only has its limitations [18]. In particular, it fails to yield the superlinear scaling of the diffusion coefficient with temperature [18]. Clearly, an alternative scheme must be sought, that would be applicable in the high-temperature regime.

Acknowledgments

The authors are grateful to the Natural Sciences and Engineering Research Council of Canada (NSERC) for financial support through the Discovery Grant 2015-04486 and to ACEnet for computational resources.

2.A Simulation details

2.A.1 The general idea

In the previous paper [18], an infinite chain was modeled as a collection of a large (~ 1000) number of oscillators with periodic boundary conditions. Such a direct simulation requires a relatively long computation time due to a large number of the degrees of freedom involved. Besides, application of periodic boundary conditions may potentially lead to an error in the determination of the diffusion coefficient [33]. In our system, this may happen for the following reason. At high temperatures, the Brownian motion proceeds predominantly via long flights, which cover many (from 10 to 10^7) lattice constant (see Section 2.7). Hence, since the periodic boundary conditions are applied, the BP may perform several rotations around the chain in a single flight and even return to its original position. This means that the local environment of the BP at the end of a flight may be unphysically correlated to

the BP environment in its beginning.

To get a more realistic simulation of a linear, as opposed to a circular, motion, as well as to reduce the overall computational effort, we devised a different type of the boundary conditions, namely, the moving stochastic boundary conditions.

As in other calculations of this type [34–36], we group the chain oscillators into three main regions: the relevant central region in immediate contact with the BP, and two outer regions, which are half-infinite chains to the left and to the right of the central region. All atoms of the central region are simulated explicitly. As for the two outer regions, only their boundary atoms that contact the central region are simulated.

We introduce two modifications into this approach. The crucial modification adopted in our treatment is that the properties of those two boundary atoms are renormalized so as to make their displacement correlation function resemble that of atoms of a half-infinite chain in the absence of a BP. The second step is to work out a way to make the truncated chain of the central region move together with the BP so as to correctly mimic its motion on an infinite chain.

2.A.2 Chain truncation

2.A.2.1 Renormalization of the boundary oscillators.

First, let us consider the oscillator chain (2.4) without the BP. In [18], the correlation function of the chain was derived,

$$
\begin{aligned}
c_j(t) &:= \frac{\langle u_0(0)\, u_j(t)\rangle_0}{T} \\
&= \frac{e^{-t/\tau}}{2\pi}\int_{-\pi}^{\pi} d\theta\, \frac{\cos(j\theta)}{\tilde{K}(\theta)}\left(\cos\big(\Omega(\theta)t\big) + \frac{\sin\big(\Omega(\theta)t\big)}{\Omega(\theta)\tau}\right) , \\
\tau &= \frac{2m}{\gamma} , \quad \tilde{K}(\theta) = \kappa_0 + 2\kappa_1(1-\cos\theta) , \\
\Omega(\theta) &= \sqrt{\frac{\tilde{K}(\theta)}{m} - \frac{1}{\tau^2}} ,
\end{aligned}
\tag{2.30}
$$

where $\langle \ldots \rangle_0$ means thermal average at $\varepsilon = 0$. The so defined correlation functions $c_j(t)$ are temperature-independent.

We would like to replace the infinite chain (2.4) with a finite one consisting of a reasonably small number n of oscillators. The correlation function of the oscillators in the middle of the truncated chain must remain as close as possible to the infinite-chain expression (2.30). For this, the equations of motion of the oscillators bearing the labels $j = 2, \ldots, n-1$ are kept the same as in (2.4), while the properties of the leftmost ($j = 1$) and rightmost ($j = n$) oscillators are renormalized so as to approximately account for the effect of the two semi-infinite chains (with $j = \ldots, -1, 0$ and $j = n+1, n+2, \ldots$) that are removed from the picture:

$$
\begin{aligned}
m\ddot{u}_1 &= -\kappa_0' u_1 - \kappa_1(u_1 - u_2) - \gamma'\dot{u}_1 + \sqrt{2\gamma' T}\,\xi_1(t) , \\
m\ddot{u}_j &= -\kappa_0 u_j - \kappa_1(2u_j - u_{j-1} - u_{j+1}) \\
&\qquad - \gamma\dot{u}_j + \sqrt{2\gamma T}\,\xi_j(t) , \quad j = 2, \ldots n-1 , \\
m\ddot{u}_n &= -\kappa_0' u_n - \kappa_1(u_n - u_{n-1}) - \gamma'\dot{u}_n + \sqrt{2\gamma' T}\,\xi_n(t) .
\end{aligned}
\tag{2.31}
$$

The oscillators 1 and n are the boundary oscillators.

To choose their renormalized pinning stiffness κ_0' and the damping coefficient γ' oscillators, consider the simplest limiting case $n = 1$, i.e. just one oscillator with damping coefficient and pinning stiffness denoted as $\tilde{\gamma}$ and $\tilde{\kappa}_0$:

$$m\ddot{u} = -\tilde{\kappa}u - \tilde{\gamma}\dot{u} + \sqrt{2\tilde{\gamma}T}\xi(t) \ . \tag{2.32}$$

We try to choose the renormalized parameters $\tilde{\gamma}$ and $\tilde{\kappa}$ so as to faithfully reproduce those aspects of the autocorrelation function (2.30) (with $j = 0$) that are most relevant to the oscillator's response to a weak external perturbation. Hence, we demand that the dynamics (2.32) had the same value of the equal-time correlation function and the integral of the correlation function as a representative oscillator in an infinite chain:

$$\begin{aligned} &\frac{\langle u^2 \rangle}{T} \stackrel{!}{=} C_0 := c_0(0) \ , \\ &\int_0^\infty dt \frac{\langle u(0)u(t)\rangle_0}{T} \stackrel{!}{=} B_0 := \int_0^\infty dt\, c_0(t) \ . \end{aligned} \tag{2.33}$$

It is the parameters C_0 and B_0 that determine the renormalized potential and the damping coefficient in the Langevin description [18,37].

Multiplication of (2.32) with $u(0)$ and averaging over noise and over the initial position gives us the equation of motion for the autocorrelation function of the stochastic oscillator's coordinate:

$$m\frac{d^2\langle u(t)u(0)\rangle}{dt^2} = -\tilde{\kappa}\langle u(t)u(0)\rangle - \tilde{\gamma}\frac{d\langle u(t)u(0)\rangle}{dt} \ , \tag{2.34}$$

with the initial conditions

$$\langle u^2 \rangle = \frac{T}{\tilde{\kappa}} \ , \quad \left.\frac{d\langle u(t)u(0)\rangle}{dt}\right|_{t=0} = 0 \ . \tag{2.35}$$

The first initial condition immediately gives the renormalized pinning stiffness:

$$\tilde{\kappa} \stackrel{!}{=} \frac{1}{C_0} \ . \tag{2.36}$$

After integrating (2.34) over time from 0 to ∞, we find the renormalized damping coefficient:

$$\tilde{\gamma} = B_0 \tilde{\kappa}^2 = \frac{B_0}{C_0^2} \ . \tag{2.37}$$

The parameters B_0 and C_0 can be found from (2.30), see [18]:

$$C_0 = \frac{1}{\sqrt{\kappa_0^2 + 4\kappa_0\kappa_1}} \ , \quad B_0 = \gamma \frac{\kappa_0 + 2\kappa_1}{(\kappa_0^2 + 4\kappa_0\kappa_1)^{3/2}} \ . \tag{2.38}$$

The dynamics of an isolated stochastic oscillator (2.32) resembles that of a "representative" oscillator of the full chain if its parameters are chosen according to (2.36)-(2.37).

The renormalized damping coefficient $\tilde{\gamma}$ and pinning stiffness $\tilde{\kappa}$ differ from the "bare" counterparts γ, and κ_0 due to the effect of the two semi-infinite chains that are connected to our representative oscillator from the left and from the right. Each of those two half-chains has its own damping and elasticity, which add up to the "bare" values κ_0 and γ of the representative oscillator.

Focusing now on the end oscillators in (2.31) (see Fig. 2.1), where the first and the last oscillators are coupled to just one semi-infinite chain, we conclude that the renormalized parameters should be chosen as

$$\begin{aligned} \kappa_0' &= \kappa_0 + \frac{\Delta\kappa_0}{2} \ , \quad \Delta\kappa_0 = \tilde{\kappa} - \kappa_0 \ , \\ \gamma' &= \gamma + \frac{\Delta\gamma}{2} \ , \qquad \Delta\gamma = \tilde{\gamma} - \gamma \ . \end{aligned} \tag{2.39}$$

2.A.2.2 Numerical validation.

Before we proceed, we would like to show that the scheme described above serves its purpose. In Figs. 2.6(a) and Fig. 2.6(b), the exact autocorrelation function $c_0(t)$ from (2.30) is compared to the autocorrelation function in a truncated chain consisting of $n = 20$ oscillators, obtained by numerical simulation of (2.31) supplemented by (2.36)-(2.37).

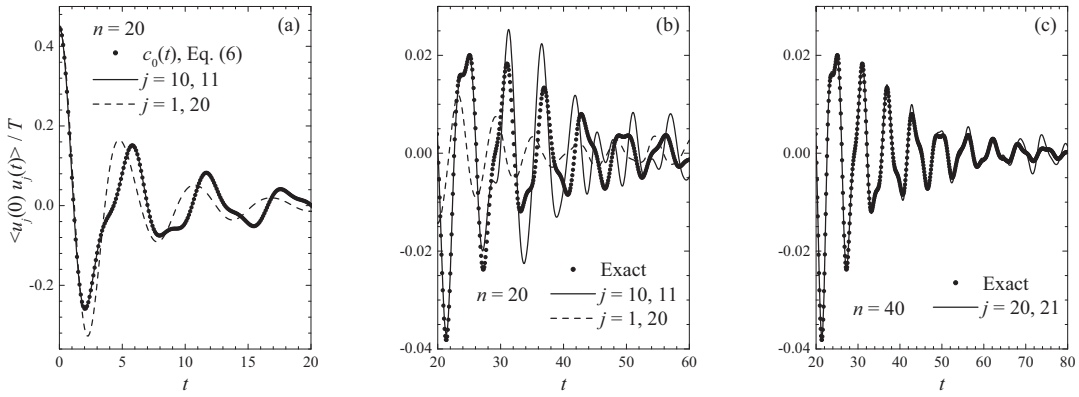

Figure 2.6 – Autocorrelation function $c_0(t) = \langle u_j(0)\, u_j(t)\rangle_0 /T$ for the parameter values $\kappa_0 = \kappa_1 = 1$, $m = 1$, $\gamma = 0.1$, as obtained according to (2.30) (circles) and by numerical simulations of a truncated chain consisting of [(a) and (b)] 20 and (c) 40 oscillators. The numerical autocorrelation function of the renormalized first and last oscillators is shown as dashed line in panels (a) and (b), and the curve for the two oscillators in the middle of the truncated chain ($j = 10, 11$) is shown as a solid line. The solid curve in panel (c) shows the autocorrelation function of the two central oscillators in a longer truncated chain of 40 oscillators.

For the renormalized first and last oscillators, the initial agreement of $\langle u_j(0)u_j(t)\rangle/T$ with the exact curve $c_0(t)$ persists only until $t \approx 1.5$ time units, after which the agreement is only qualitative, see Fig. 2.6(a).

On the other hand, for the oscillators $j = 10$ and 11 in the middle of the chain, the agreement persists up to the time $t = 25$, i.e. the first four oscillation periods of $c_0(t)$, see Fig. 2.6 (b). Doubling the number of oscillators in the truncated chain to $n = 40$ makes the agreement at large times almost perfect (see Fig. 2.6 (c)). But at large times, the value of the autocorrelation function drops to only a few per cent of the initial value $c_0(0)$; hence, the discrepancy between the exact and numerical curves at large times should have a negligibly small effect on the dynamics of the BP.

2.A.3 Moving stochastic boundary

We now place the BP in the middle of a truncated chain containing a reasonably small number n of oscillators. If the BP were confined to a small region near the middle of the truncated chain (2.31) by a static external potential, then its dynamics would be statistically indistinguishable from the dynamics of a BP in contact with an infinite chain. But we are interested in the free diffusion of the BP; hence, the truncated chain must somehow move together with it.

To achieve this, we adopt the following algorithm. Let x_c be the position of the chain center in mechanical equilibrium. It is expressed as an integer multiple of the lattice constant a if the truncated chain consists of an odd number n of oscillators and as a half-integer multiple of a if n is even. Then, the position of the jth oscillator can be measured relative to x_c as

$$x_j = x_c + a\left(j - \frac{n+1}{2}\right) + u_j \ , \quad j = 1, \ldots, n \ . \tag{2.40}$$

Let us place the BP within an interval of width a centered at x_c:

$$x_c - a/2 < X < x_c + a/2 \ . \tag{2.41}$$

As the particle moves, it will eventually cross one of the boundaries of this interval. If the BP crosses the right boundary at $x_c + a/2$, the following steps are carried out:

(i) The position of the center is increased by one lattice constant, $x_c \to x_c + a$.

(ii) A cyclic permutation of the oscillator labels is performed, $j \to (j-1)(1-\delta_{j1}) + n\delta_{j1}$, i.e. all oscillator labels are decreased by one and the formerly first oscillator becomes the nth one.

(iii) The velocity of the new last oscillator $\dot{u}_n$ is reset to a Gaussian random variable with zero mean and the variance $\sqrt{T/m}$.

(iv) The coordinate of the new n'th oscillator is reset to

$$u_n \to z u_{n-1} + r\sqrt{1-z^2}\ , \tag{2.42}$$

where r is an independent Gaussian random variable with zero mean and the same variance as that of a representative oscillator of a SHOC without the BP:

$$\langle r^2 \rangle = TC_0 = \frac{T}{\tilde{\kappa}} = \frac{T}{\sqrt{\kappa_0^2 + 4\kappa_0\kappa_1}}\ . \tag{2.43}$$

This ensures that also $\langle u_n^2 \rangle = z^2 \langle u_{n-1}^2 \rangle + (1-z^2)\langle r^2 \rangle = \langle r^2 \rangle = T/\tilde{\kappa}$. The constant z is chosen so as to make sure that the equal-time correlation between the newly formed nth oscillator with the previous $(n-1)$'th one has the correct value from (2.30):

$$\langle u_n u_{n-1} \rangle = z\langle u_{n-1}^2 \rangle = zTC_0 \stackrel{!}{=} Tc_1(0)\ . \tag{2.44}$$

The value of $c_1(0)$ has been determined in the appendix of [18]. Hence

$$z = \frac{\alpha - \sqrt{\alpha^2 - 4}}{2}\ ,\quad \alpha = 2 + \frac{\kappa_0}{\kappa_1}\ . \tag{2.45}$$

If the BP crosses the left boundary of the interval (2.41), then the steps are similar:

(i) The position of the truncated chain center is decreased by one lattice constant, $x_c \to x_c - a$.

(ii) A cyclic permutation of the oscillator labels $j \to (j+1)(1-\delta_{jn}) + \delta_{jn}$ is performed.

(iii) The velocity of the new first oscillator is randomly chosen from the Maxwellian probability distribution $\propto e^{-m\dot{u}_1^2/(2T)}$.

(iv) The displacement of the new first oscillator is reset to $u_1 \to z u_2 + r\sqrt{1-z^2}$, where r is a zero-mean Gaussian random variable with the variance from (2.43) and z is given by (2.45).

The simulations were performed for the parameters from Eq. (2.6). The truncated chain consisted of $n = 21$ oscillators if the SHOC oscillators were interacting ($\kappa_1 = 1$), and of

$n = 5$ oscillators if they were independent ($\kappa_1 = 0$). In the case $\kappa_1 = 1$, out of the 21 truncated chain oscillators, 19 formed the central region and 2 outer oscillators were renormalized. For $\kappa_1 = 0$, no renormalization of the outer oscillators is necessary, because in this case $\kappa_0' = \kappa_0$ and $\gamma' = \gamma$, as follows from Eqs. (2.36)-(2.39). The number n was chosen to be odd in order for the BP to stay in contact with the central oscillator during its rest phases; otherwise, the steps (i)-(iv) described above would have to be performed much more frequently. The results reported in this paper did not change if the truncated chain length n was increased by a factor of 2, i.e. to $n = 41$ for $\kappa_1 = 1$ and to $n = 11$ for $\kappa_1 = 0$.

2.B Numerical evaluation of the diffusion coefficient

We employ the specifics of the BP trajectory, which consists of the alternating rest and flight phases, see Fig. 2.7(a). Numerically, the two phases can be easily distinguished by observing the distance traveled by the BP between two successive turning points marked by a sign change of the velocity. If this distance is smaller than the lattice constant, the particle is resting; otherwise, it is flying. It is convenient to measure the duration of the rest phases as the number of times ν_r the BP changes its direction of motion while remaining bound to one of the chain oscillators. The smallest value of $\nu_r = 1$ corresponds to a reflection event of the BP by an oscillator, see Fig. 2.7(a).

Recording the full trajectory with a reasonably small time step, e.g. every 0.1 time units, made the output file size prohibitively large, not to mention the fact that data processing would then be more complicated numerically. Therefore, only the most pertinent data was recorded into a file in the course of each simulation, namely, the duration of the rest phases that separate successive flights, the number of oscillation half-periods in each rest phase, the duration of flights, and the flight length measured in integer multiples of the lattice

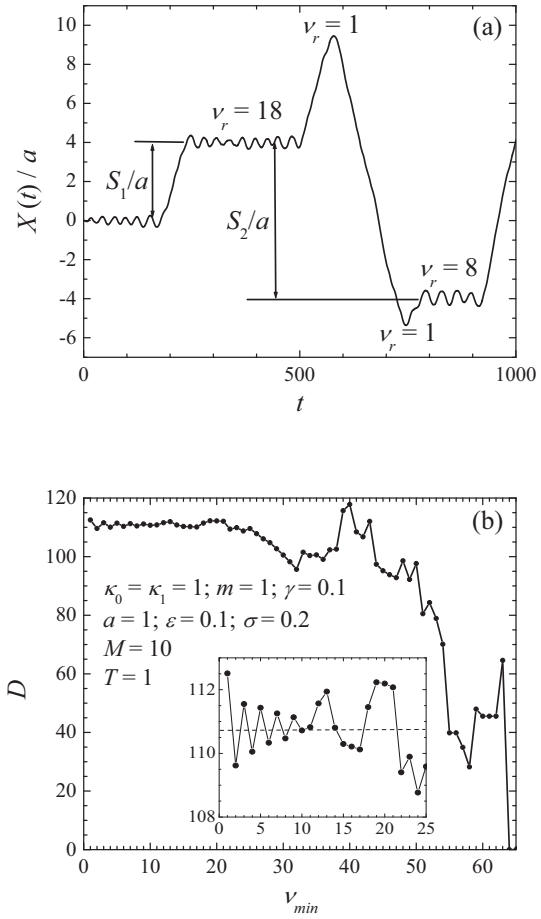

Figure 2.7 – (a) A representative BP trajectory showing the first few rest and flight phases, as well as the first two segments $S_1 = 4a$ and $S_2 = -8a$ that appear in equation (2.49). The segment S_1 consists of a single flight, whereas S_2 consists of three flights of length L equal to $4a$, $-14a$, and $2a$. The flights are separated by the rest phases whose duration ν_r is measured as the number of times the BP changes the sign of its velocity. (b) The numerical diffusion coefficient obtained according to (2.49) for the chain parameters indicated in the legend as a function of the duration ν_r of the rest phases that separate two consecutive segments. The inset shows the initial part of the same graph.

constant:

$$l = \lfloor L/a \rfloor \ , \tag{2.46}$$

where L is the actual flight length, i.e. the distance (greater than a) traveled by the BP between two successive turning points marked by the velocity sign change. Each of the resulting files, consisting of 4 columns with these parameters, had the size of ca. 570 kB.

For each temperature probed, 25 stochastic trajectories were simulated in parallel with different initial seeds of the random number generator. Each simulation was run until the BP performed a large number of $2 \cdot 10^4$ flights, giving $5 \cdot 10^5$ flights in total.

The total displacement of the BP after a long observation time t_{obs} may be split into segments,

$$\Delta X(t) = \sum_k S_k \ . \tag{2.47}$$

The duration of each segment does not have to be the same, and each segment does not necessarily represent the BP displacement in a single flight, see Fig. 2.7(a). What is important that the displacements in any two consecutive segments are uncorrelated with each other. More precisely, we demand that

$$|\langle S_k S_{k+1} \rangle| \ll \langle S_k^2 \rangle \ . \tag{2.48}$$

Then, the correlations $\langle S_k S_{k'} \rangle$ with $k \neq k'$ can be neglected, and the diffusion coefficient is expressed as

$$D = \frac{\langle S^2 \rangle}{2(\langle t_r \rangle + \langle t_f \rangle)} = \frac{\sum_k \langle S_k^2 \rangle}{2t_{obs}} \ . \tag{2.49}$$

where t_r and t_f are the durations of rest and fly phases, respectively, and averaging is performed with respect to many rest-and-fly phases observed in the simulations.

It remains to decide on how to choose the segments S_k so as to fulfill the condition (2.48). Clearly, if two such segments are separated by a very brief rest phase, then they might still be correlated with each other. Therefore, we identify the segments S_k with the distance traveled by the BP in one or more successive flights that are separated from each other by the rest phases of duration smaller than some preset minimal interval ν_{min}.

Correspondingly, the duration of the rest phases that separate two successive segments should exceed ν_{min}. For example, in Fig. 2.7(a), ν_{min} is an integer between 2 and 8. Hence, the first segment S_1 consists of just one flight from 0 to $4a$; the segment S_2 is formed by 3 flights with the net displacement from $4a$ to $-4a$, as they are separated from each other by turning points with $\nu_r = 1$.

Figure 2.7(b) shows the so obtained diffusion coefficient vs. ν_{min} for a BP/SHOC parameter set $\kappa_1 = 1$, $\varepsilon = 0.1$ at the temperature $T = 1$. It is seen that the diffusion coefficient initially shows very small variations with ν_{min}, see inset in Fig. 2.7(b). Especially for $\nu_{min} \leq 10$, the diffusion coefficient (2.49) exhibits decaying oscillations around the value of about 111. The size of those oscillations is only about 1 % of this value. We believe that these oscillations are due to the $\langle S_k S_{k'} \rangle$ terms with $k \neq k'$ neglected in (2.49).

Increasing the waiting time ν_{min} makes the curve in Fig. 2.7(b) quite irregular due to statistical reasons, as increasing the minimal waiting time results in a significant decrease of the total number of segments S_k in the trajectory. The overall trend is that the calculated diffusion coefficient decreases with ν_{min} down to $D = 0$ at $\nu_{min} > 64$. This value is immediately understood from Eq. (2.49): if ν_{min} is too high, then only one segment is present in the trajectory with a not necessarily big overall displacement. However, the simulation time t_{obs} is long, resulting in a very small ratio (2.49).

We conclude that the value of ν_{min} does not have to be very big; typically, it suffices to set ν_{min} to be of the order of a few oscillation periods of the BP in a rest phase. The results presented below are obtained for $\nu_{min} = 10$.

Bibliography

[1] A. Kaffashnia, M. Evstigneev. Scaling and universality in Brownian motion on a stochastic harmonic oscillator chain. *Phys.Rev. E*, **105**, 064134, (2022).

[2] L. Kadanoff. Scaling and universality in statistical physics. *Physica A*, **163**, 1, (1990).

[3] M.E. Fisher. Scaling, Universality and Renormalization Group Theory. In: F.J.W. Hahne (ed.) *Critical Phenomena. Lecture Notes in Physics*, vol. 186 (Springer, Berlin, Heidelberg), (1983).

[4] S. Kumar, S. Sarkar, and B. Bagchi. Microscopic origin of breakdown of Stokes–Einstein relation in binary mixtures: Inherent structure analysis. *J. Chem. Phys.*, **152**, 164507, (2020).

[5] V. Dubey and S. Daschakraborty. Breakdown of the Stokes–Einstein Relation in Supercooled Water/Methanol Binary Mixtures: Explanation Using the Translational Jump-Diffusion Approach *J. Phys. Chem. B*, **124**, 10398, (2020).

[6] V. Dubey, S. Erimban, S. Indra, and S. Daschakraborty. Understanding the origin of the breakdown of the Stokes–Einstein relation in supercooled water at different temperature–pressure conditions. *J. Phys. Chem. B*, **123**, 10089, (2019).

[7] L. Costigliola, D.M. Heyes, T.B. Schroder, and J.C. Dyre. Revisiting the Stokes-Einstein relation without a hydrodynamic diameter. *J. Chem. Phys.*, **150**, 021101, (2019).

[8] S. Wei, Z. Evenson, M. Stolpe, P. Lucas, and C.A. Angell. Breakdown of the Stokes-Einstein relation above the melting temperature in a liquid phase-change material. *Sci. Adv.*, **4**, eaat8632, (2018).

[9] S. Pan, Z.W. Wu, W.H. Wang, M.Z. Li, and L. Xu. Structural origin of fractional Stokes-Einstein relation in glass-forming liquids. *Sci. Rep.*, **7**, 1–9, (2017).

[10] N. Ohtori, S. Miyamoto, and Y. Ishii. Breakdown of the Stokes-Einstein relation in pure Lennard-Jones fluids: From gas to liquid via supercritical states. *Phys. Rev. E*, **95**, 052122, (2017).

[11] C.H. Li, Y.W. Luan, X.J. Han, and J.G. Li. Structural aspects of the Stokes-Einstein relation breakdown in high temperature melts. *J. Non-Cryst. Solids*, **458**, 107, (2017).

[12] H.R. Schober and H.L. Peng. Heterogeneous diffusion, viscosity, and the Stokes-Einstein relation in binary liquids. *Phys. Rev. E*, **93**, 052607, (2016).

[13] P. Charbonneau, Y. Jin, G. Parisi, and F. Zamponi. Hopping and the Stokes–Einstein relation breakdown in simple glass formers. *Proc. Nat. Acad. Sci.*, **111**, 15025, (2014).

[14] E. Schrödinger. Zur dynamik elastisch gekoppelter punktsysteme. *Ann. Phys.*, **44**, 916, (1914).

[15] G.W. Ford, M. Kac and P. Mazur. Statistical mechanics of assemblies of coupled oscillators. *J. Math. Phys.*, **6**, 504, (1965).

[16] G.W. Ford, J.T. Lewis, and R.F. O'Connell. Independent oscillator model of a heat bath: exact diagonalization of the Hamiltonian. *J. Stat. Phys.*, **53**, 439, (1988).

[17] A.V. Plyukhin. Fractional Langevin equation from damped bath dynamics. *Phys. Rev. E*, **99**, 052125, (2019).

[18] M. Evstigneev M and A. Al-Haidari. Brownian motion on a stochastic harmonic oscillator chain: limitations of the Langevin equation. *J. Phys. A: Math. Theor.*, **52**, 055001, (2019).

[19] G. Basile and S. Olla. Energy diffusion in harmonic system with conservative noise. *J. Stat. Phys.*, **155**, 1126, (2014).

[20] M. Jara, T. Komorowski, and S. Olla. Superdiffusion of energy in a chain of harmonic oscillators with noise. *Commun. Math. Phys.*, **339**, 407, (2015).

[21] A.V. Plyukhin and J. Schofield. Trapping, reflection, and fragmentation in a classical model of atom-lattice collisions. *Phys. Rev. E.*, **65**, 026603, (2002).

[22] O.V. Gendelman and A.V. Savin. Normal heat conductivity of the one-dimensional lattice with periodic potential of nearest-neighbor interaction. *Phys. Rev. Lett.*, **84**, 2381, (2000).

[23] J.R. Chaudhuri, P. Chaudhury, and S. Chattopadhyay. Harmonic oscillator in presence of nonequilibrium environment. *J. Chem. Phys.*, **130**, 234109, (2009).

[24] A.A. Silvius, P.E. Parris, and S. De Bièvre. Adiabatic-nonadiabatic transition in the diffusive Hamiltonian dynamics of a classical Holstein polaron. *Phys. Rev. B*, **73**, 014304, (2006).

[25] P. Lafitte, P.E. Parris, and S. De Bièvre. Normal transport properties in a metastable stationary state for a classical particle coupled to a non-Ohmic bath. *J. Stat. Phys.*, **132**, 863, (2008).

[26] Y. Sang, M. Dubé, and M. Grant. Dependence of friction on roughness, velocity, and temperature. *Phys. Rev. E*, **77**, 036123, (2008).

[27] C. Apostoli et al. Velocity dependence of sliding friction on a crystalline surface. *Beilstein J. Nanotechnol.*, **8**, 2186, (2017).

[28] M. Melillo, F. Zhu, M.A. Snyder, and J. Mittal. Water transport through nanotubes with varying interaction strength between tube wall and water. *J. Phys. Chem. Lett.*, **2**, 2978, (2011).

[29] J. Geng et al., Stochastic transport through carbon nanotubes in lipid bilayers and live cell membranes. *Nature*, **514**, 612, (2014).

[30] D. Huang, Y. Chen, and K.A. Fichthorn. A molecular-dynamics simulation study of the adsorption and diffusion dynamics of short n-alkanes on Pt(111). *J. Chem. Phys.*, **101**, 11021, (1994).

[31] W.D. Luedtke and U. Landman. Slip diffusion and Levy flights of an adsorbed gold nanocluster. *Phys. Rev. Lett.*, **82**, 3835, (1999).

[32] B. Yoon, W.D. Luedtke, J. Gao, and U. Landman. Diffusion of gold clusters on defective graphite surfaces. *J. Phys. Chem.*, **107**, 5882, (2003).

[33] S. von Bülow, J.T. Bullerjahn, and G. Hummer. Systematic errors in diffusion coefficients from long-time molecular dynamics simulations at constant pressure. *J. Chem. Phys.*, **153**, 021101, (2020).

[34] L. Kantorovich. Generalized Langevin equation for solids. I. Rigorous derivation and main properties. *Phys. Rev. B*, **78**, 094304, (2008).

[35] L. Kantorovich and N. Rompotis. Generalized Langevin equation for solids. II. Stochastic boundary conditions for nonequilibrium molecular dynamics simulations. *Phys. Rev. B*, **78**, 094305, (2008).

[36] A. Benassi, A, Vanossi, G.E. Santoro, and E. Tosatti. Optimal energy dissipation in sliding friction simulations. *Tribol. Lett.*, **48**, 41, (2012).

[37] M. Evstigneev and P. Reimann. Langevin equation for a system nonlinearly coupled to a heat bath. *Phys. Rev. B*, **82**, 224303, (2010).

Chapter 3

Origin of the dispersionless transport in spite of thermal noise

In this chapter, we present our subsequent work [1] by Amir Kaffashnia and Mykhaylo Evstigneev, with kind permission of the publishers of Physical Review E. The paper can be accessed through the DOI link: 10.1103/PhysRevE.104.054113.

3.1 Abstract

The "dispersionless transport" of a weakly damped Brownian particle in a tilted periodic potential is defined by (i) a plateau of the particle's coordinate dispersion extending over a very broad time interval and (ii) by the impossibility to measure the diffusion coefficient within this plateau region. While the first part of this definition has been explained in the literature, the second part has been thought to follow from (i). Here, the impossibility to measure the diffusion coefficient is shown to be actually due to the wild fluctuations of the dispersion itself in the plateau region. An expression for the time scale over which a reliable determination of the diffusion coefficient is possible is derived. A procedure that allows accurate determination of the diffusion coefficient by observing the particle trajectory only

within a small part of the plateau region is suggested and shown to be feasible by numerical simulations of a weakly damped Brownian particle in a tilted washboard potential.

3.2 Introduction

When combined with non-linearity, noise may produce a number of surprising effects in dynamical systems out of thermal equilibrium. Examples include stochastic resonance [2], ratchet effect [3], absolute negative mobility [4–7], and transport against temperature gradient [8] to name but a few.

To such effects belongs the "dispersionless transport", first reported by Lindenberg et al. [9]. They considered a weakly damped Brownian particle in a periodic potential tilted by a constant force. It is textbook knowledge that after an initial transient process, the dispersion of the particle's coordinate should increase linearly in time, and the rate of its increase is the diffusion coefficient multiplied by twice the dimensionality of the system. But instead, it was observed in [9] that the dispersion reached a plateau and stayed constant for a very long time. For some parameter values, the duration of this plateau was much longer than a reasonable computation time, making it impossible to determine the diffusion coefficient from the simulations [9].

Later, the effect of "dispersionless transport" has been reported in a ratchet system [10,11], for the time-periodic force of zero mean value [12] and for a combination of dc and ac forces [13], as well as for Brownian motion in a random potential [14].

Although the explanation of this effect proposed in [9] is intuitively appealing, some aspects of the "dispersionless transport" remain unclear. In particular, it is well understood why the plateau value of the dispersion is much larger than the linearly increasing term due to diffusion [9]. But however big, the dispersion plateau value is just a constant, i.e. the dispersion should still increase linearly in time, and the diffusion coefficient should still be

obtainable from the dispersion vs. time plot by linear fitting in the plateau regime. Yet, this is not the case in practice.

Here, we expand the interpretation from [9] and explain this by a combination of two factors: the large value of the initial dispersion in the plateau region [9] and by the fact that in simulations, averaging is necessarily performed over a large, but finite number of stochastic trajectories. The latter aspect has been overlooked in the literature, but is crucial in understanding of the impossibility to measure the diffusion coefficient in the plateau regime. Finally, we introduce a simple modification of the measurement procedure that allows measuring the diffusion coefficient by observing the system's dynamics in the plateau region over a relatively short time scale.

3.3 "Dispersionless transport" in a tilted periodic potential

3.3.1 Dispersion plateau

Consider a weakly damped Brownian particle in a tilted one-dimensional periodic potential $U(x)$ under the action of a constant force F. The particle dynamics is governed by the Langevin equation

$$\begin{aligned} m\ddot{x}_t &= -U'(x_t) + F - \gamma\dot{x}_t + \sqrt{2\gamma T}\xi(t) \ , \\ U(x) &= -\frac{U_0}{2} cos \frac{2\pi x}{a} \ , \end{aligned} \tag{3.1}$$

where x_t is the coordinate of the particle at time t, and the prime and the overdot denote spacial and time derivatives, respectively. The potential $U(x)$ has corrugation depth U_0 and periodicity a; m and γ are the mass and damping coefficient, respectively, T is the temperature, and $\xi(t)$ is unbiased Gaussian white noise of unit strength: $\langle\xi(t)\rangle = 0$, $\langle\xi(t)\xi(t')\rangle = \delta(t-t')$. We are interested in the evolution of the particle dispersion, defined as

$$\sigma_x^2(t) := \langle x_t^2\rangle - \langle x_t\rangle^2 \ . \tag{3.2}$$

In the long-time limit, it should increase linearly in time

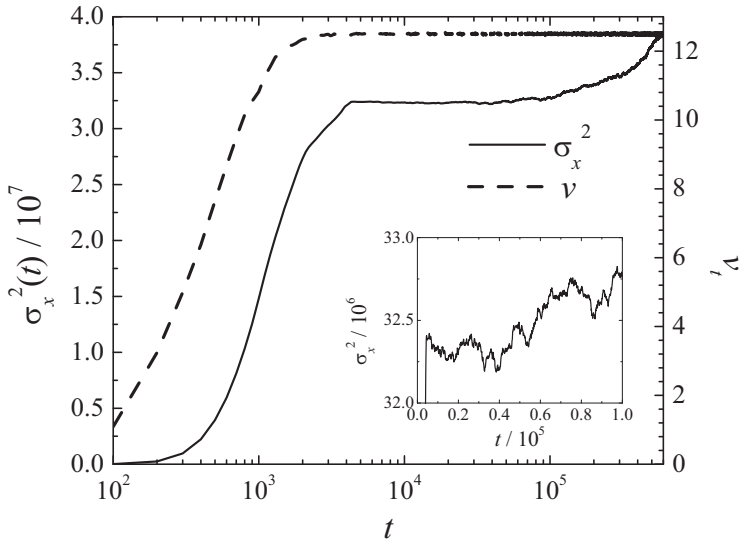

Figure 3.1 – Dispersion (3.2) (solid line) and average velocity $v_t = \langle \dot{x}_t \rangle$ (dashed line) of a Brownian particle in a tilted washboard potential (3.1) with the parameters used in [9]: $m = 1$, $U_0 = 1$, $a = 1$, $\gamma = 0.04$, $T = 0.2$, and $F = 0.5$. The curves are obtained by simultaneously simulating equation (3.1) for $N = 1000$ independent Brownian particles with the initial conditions $x_0 = \dot{x}_0 = 0$ and averaging over 1000 trajectories. The inset shows the dispersion vs. time curve in the plateau region on the linear scale.

$$\sigma_x^2(t) = 2Dt \ , \tag{3.3}$$

where D is the diffusion coefficient. We performed simulations of equation (3.1) for the parameters specified in the caption to Fig. 3.1 with the initial conditions

$$x_0 = \dot{x}_0 = 0 \ , \tag{3.4}$$

It is clear that the dispersion has a plateau, where it practically does not change in time, see Fig. 3.1. One may suspect that its constancy might be due to the use of the logarithmic

scale on the time axis, but using the linear scale does not reveal a linear increase according to (3.3), see inset in Fig. 3.1. Hence, this plateau is often termed "dispersionless transport" in the literature [9–14].

3.3.2 Interpretation of the dispersion plateau

The interpretation of this effect offered in [9] is as follows. Suppose that initially the particle found itself near some minimum of the total potential $U(x)$ - Fx with $|F| < max_x|U'(x)|$. Its escape from that potential well is described by Kramers' theory. The mean escape time τ_0 from the potential well depends on the shape of the potential near the minimum, the force, the damping, the temperature, and, most importantly, on the barrier height ΔU that separates the current potential minimum from the next one [15]. After escape, the particle moves with a constant velocity F/γ. The distribution of the escape times τ is exponential and is proportional to $e^{-\tau/\tau_0}$. Hence, the initial width of the spacial probability distribution to find the particle can be estimated as $\sigma^2_{plateau} \sim (F\tau_0/\gamma)^2$. As the particle moves after the escape, its spacial dispersion is

$$\sigma_x^2 \approx \sigma^2_{plateau} + 2Dt \ . \tag{3.5}$$

From this, it is concluded [9] that the duration of the "dispersionless" phase is

$$t_{plateau} = \sigma^2_{plateau}/2D \ . \tag{3.6}$$

Because the mean escape time is proportional to the Kramers-Arrhenius factor [15], $\tau_0 \propto e^{\Delta U/T}$ and can be very large for $T \ll \Delta U$, the initial dispersion $\sigma^2_{plateau} \propto e^{2\Delta U/T}$ may also be very large, implying very long duration of the "dispersionless" phase.

Based on this interpretation, the authors of [9] identified thermal fluctuations, weak damping, periodicity of the potential $U_0(x)$, and the presence of a non-zero bias such that $|F| < max_x|U'(x)|$ as necessary conditions for the onset of the non-dispersive regime.

3.4 Dispersion fluctuations and diffusion coefficient measurement in the plateau region

3.4.1 Dispersion plateau of a free Brownian particle

In fact, the above general argument from [9] can be used to predict a dispersion plateau in *any* system where the diffusion proceeds in two stages: a fast initial stage that results in a broad initial dispersion of the coordinate to a large value $\sigma^2_{plateau}$, and slow normal diffusion that follows the initial spread. For example, a plateau can be observed even if the dynamics (3.1) is simplified to

$$m\ddot{x}_t = -\gamma\dot{x}_t + \sqrt{2\gamma T}\xi(t) \ , \tag{3.7}$$

provided the initial conditions are chosen in a special way. Namely, we place initially all particles at $x_0 = 0$, but we assume that the initial temperature of our particles was very high relative to the temperature of the environment: $T_0 \gg T$. Then, the initial distribution of the particle velocity $v_0 = \dot{x}_0$ is

$$P(v_0) \propto e^{-mv_0^2/2T_0} \ . \tag{3.8}$$

Initially, the particles cool down to the environment temperature T. In this transient process, the particle's velocity $v_t = \dot{x}_t$ can be decomposed into an exponentially decaying part (the homogeneous solution of Eq. (3.7)) and the noisy part (the particular solution of this equation): $v_t = e^{-\gamma t/m}v_0 + \Delta v_t$ where Δv_t describes the diffusive process with the diffusion coefficient $D = T/\gamma$. As the particle cools down, the coordinate dispersion rapidly increases until it reaches the rather high value

$$\sigma^2_{plateau} = \int dv_0 P(v_0)\left(\int_0^\infty dt v_0 e^{-\gamma t/m}\right)^2 = \frac{T_0 m}{\gamma^2} \ , \tag{3.9}$$

as can be obtained from the identities $\int_0^\infty dt e^{-\gamma t/m} = m/\gamma$ and $\int dv_0 P(v_0) v_0^2 = T_0/m$.

After the transient cool-down process is over, normal diffusion with $d\sigma_x^2(t)/dt = 2D$, $D = T/\gamma$ begins. This expectation is confirmed by the numerical simulations of equation (3.7) with $m = \gamma = T = D = 1$, see Fig. 3.2 showing the dispersion vs. time for two initial temperatures: $T_0 = 10^4$ (lower curve, left inset) and $T_0 = 10^8$ (upper curve, right inset). For the smaller initial temperature, $\sigma^2_{plateau} = 10^4$ and $t_{plateau} = 5.10^3$, in full agreement with Eq. (3.6). For the higher initial temperature, the duration of the plateau predicted by Eq. (3.6), $t_{plateau} = 5.10^7$, is too long to reach the increasing part of the curve within a reasonable computation time.

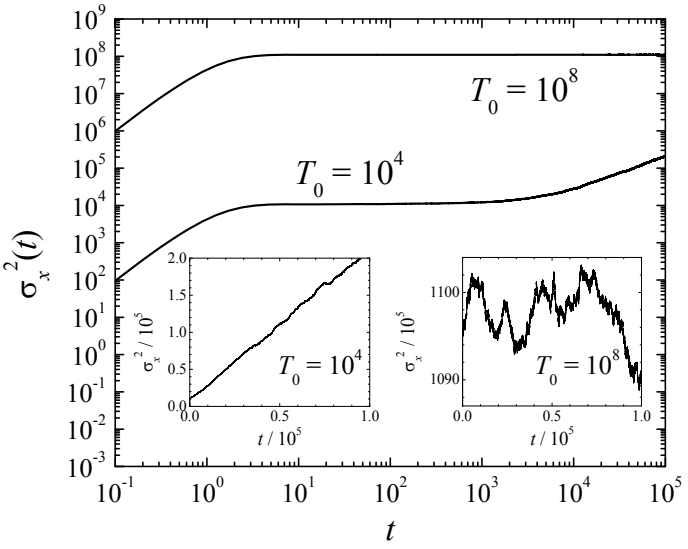

Figure 3.2 – Dispersion vs. time, as obtained from the simulations of equation (3.7) with $m = \gamma = T = 1$ and the initial temperatures $T_0 = 10^4$ (lower curve, left inset) and $T_0 = 10^8$ (upper curve, right inset). The inset shows the same plot on the linear scale.

The interpretation offered in [9] and re-iterated above only explains the existence of the plateau region, where the $2Dt$ term in Eq. (3.5) is much smaller than the first term $\sigma^2_{plateau}$. This plateau can only be observed if logarithmic scale is chosen on the time axis,

but a linear increase of $\sigma_x^2(t)$ should be observed on the linear scale, see Eq. (3.5) and the dispersion curves for $T_0 = 10^4$ in the main part and in the left inset of Fig. 3.2. What remains surprising and unexplained is that the diffusion coefficient cannot be measured by linear fitting of $\sigma_x^2(t)$ with Eq. (3.5) within the plateau region at large values of $\sigma^2_{plateau}$ when linear scale is used, see inset in Fig. 3.1 and right inset in 3.2. In the latter case, the dispersion even shows an overall decrease over a broad time scale $t \sim 10^5$, contrary to the expected linear increase with a known rate $2D = 2T/\gamma$.

Of course, such a decrease must be a spurious effect related to the wild fluctuations of the dispersion in the plateau regime. The diffusion coefficient cannot be established not because there is a dispersion plateau on the σ_x^2 vs. $\log(t)$ plot, but because, within the plateau region, the diffusive term $2Dt$ in Eq. (3.5) is submerged in these fluctuations.

3.4.2 Dispersion fluctuations

Next, we try and understand the origin of the dispersion fluctuations. Returning to the main part of Fig. 3.1, we observe that the plateau of $\sigma_x^2(t)$ begins right after the average velocity of the particle,

$$v_t = \langle \dot{x}_t \rangle \ , \tag{3.10}$$

saturates at the value $v_\infty \approx 12.5$.

Hence, we choose the origin of the time axis to be at the beginning of the dispersion plateau, assume the initial velocity of the particle to be $\dot{x}_0 = v_\infty$, and decompose the particle's coordinate into three parts:

$$x_t = x_0 + v_\infty t + y_t \ , \ \langle x_0 \rangle = y_0 = \langle \dot{y}_t \rangle = \langle y_t \rangle = 0 \ , \tag{3.11}$$

where x_0 is now a random variable. Without loss of generality, we set its average value to zero by suitably shifting the origin of the x-axis. Its dispersion is $\sigma^2_{x_0} = \sigma_x^2(0) = \sigma^2_{plateau}$.

The deviation y_t is the diffusive part of the coordinate. Its average velocity and its average value are both zero, because the average coordinate of the particle is $\langle x_t \rangle = v_\infty t$ for $t > 0$. Its dispersion should behave as

$$\sigma_y^2(t) := \langle y_t^2 \rangle - \langle y_t \rangle^2 = 2Dt \tag{3.12}$$

for sufficiently large t. This follows immediately from the relation between $\sigma_x^2(t)$, given by Eq. (3.2), and $\sigma_y^2(t)$, namely

$$\sigma_x^2(t) = \langle (x_0 + v_\infty t + y_t)^2 \rangle - (v_\infty t)^2 = \sigma_x^2(0) + \sigma_y^2(t) + 2c_t \ , \tag{3.13}$$

where we have defined the correlation function

$$c_t := \langle x_0 y_t \rangle \ . \tag{3.14}$$

In view of the initial condition $y_0 = 0$, the initial value $c_0 = 0$. If the potential $U(x)$ is flat, i.e. $U_0 = 0$, then also at later times we should have $c_t = 0$; this is so, because in the frame of reference moving with the average velocity v_∞ of the particle, positive and negative displacements y_t are equally likely. If the potential $U(x)$ is corrugated, i.e. $U_0 > 0$, the correlation function c_t may deviate from zero at $t > 0$. But even in this case, the correlation between x_0 and y_t (if any) should very quickly decay to zero on the time scale much shorter than the duration of the plateau from Eq. (3.6). Keeping this time scale in mind, we can write

$$c_t \to \langle x_0 \rangle \langle y_t \rangle = 0 \ . \tag{3.15}$$

This means that c_t should play no role in the measurements of the diffusion coefficient.

However, this kind of reasoning only applies to an idealized numerical experiment, in which an infinite number of stochastic trajectories are simulated. But in the real-life numerical simulations, averaging is performed over a large, but finite number N of stochastic

processes $x_t^{(i)}, y_t^{(i)}, i = 1, ..., N$. Correspondingly, the *numerical* correlation function, denoted with a tilde,

$$\tilde{c}_t = \frac{1}{N} \sum_{i=1}^{N} x_0^{(i)} y_t^{(i)} \ , \tag{3.16}$$

is a random variable which goes to zero only in the limit $N \to \infty$, namely

$$\tilde{c}_t \xrightarrow{N\to\infty} c_t \to 0 \ . \tag{3.17}$$

But at a finite number N of trajectories, the fluctuating part of the dispersion does not go to zero at any time $t > 0$. In fact, the size of the dispersion fluctuations increases in time.

To see this, we calculate the variance of $\tilde{c}_t$ based on the definition (3.16). We consider an infinite number of independent replicas of the numerical experiment, in each of which N stochastic trajectories are simulated, and perform averaging over those replicas, denoted as $\langle ... \rangle$ in the derivation below:

$$\begin{aligned} \sigma_{\tilde{c}}^2(t) := \langle \tilde{c}_t^2 \rangle &= \frac{1}{N^2} \sum_{i,j=1}^{N} \langle x_0^{(i)} y_t^{(i)} x_0^{(j)} y_t^{(j)} \rangle \\ &= \frac{1}{N^2} \sum_{i=1}^{N} \langle x_0^{(i)2} y_t^{(i)2} \rangle = \frac{\langle x_0^{(1)2} y_t^{(1)2} \rangle}{N} \\ &\to \frac{\langle x_0^2 \rangle \langle y_t^2 \rangle}{N} = 2Dt \frac{\sigma_x^2(0)}{N} \ , \end{aligned} \tag{3.18}$$

In the second line, we used independence of the replicas, which implies that only the terms with $j = i$ survive in the double sum. For $i \neq j$, the summands split into $\langle x_0^{(i)} y_t^{(i)} \rangle \langle x_0^{(j)} y_t^{(j)} \rangle = c_t^2 \to 0$. Because all trajectories are statistically the same, the sum in the second line contains N identical terms, each of which equals the first one. In the third line, we removed the superfluous superscript (1) and focused on the time-scale sufficient for the correlation between x_0 and y_t to be lost, allowing us to replace $\langle x_0^2 y_t^2 \rangle$ with $\langle x_0^2 \rangle \langle y_t^2 \rangle$. In the last step, we used the identities $\langle x_0^2 \rangle = \sigma_x^2(0)$ and $\langle y_t^2 \rangle = 2Dt$.

Thus, in the realistic numerical simulations, the dispersion (3.13) contains a linearly increasing part $\sigma_y^2(t) = 2Dt$ and a fluctuating part $2\tilde{c}_t$. The standard deviation of the

dispersion can be estimated as $2\sigma_{\tilde{c}}(t) = 2\sqrt{2Dt/N}\sigma_x(0)$, as follows from Eq. (3.18). Note that $\sigma_y^2(t) \sim t$ increases with time faster than $2\sigma_{\tilde{c}}(t) \sim \sqrt{t}$.

In order to measure the diffusion coefficient with a reasonable accuracy, the former must be bigger than the latter by a large number A inversely proportional to the desired accuracy of D; e.g. $A = 10$ corresponds to the accuracy of 10%. This means that the waiting time, t_D, necessary to reliably measure D can be estimated as

$$\sigma_y^2(t_D) = 2Dt_D = 2A\sigma_{\tilde{c}}(t_D) \ , \ t_D = 2A^2\frac{\sigma_x^2(0)}{ND} \ , \tag{3.19}$$

With the parameters used to build the graphs in Fig. 3.1 ($\sigma^2_{plateau} = 3.2 \ . \ 10^7, \ D = 5, \ N = 1000$) the inequality $t > t_D$ implies that the diffusion coefficient becomes measurable for the waiting times exceeding $t > 10^6$, in agreement with the simulation results. Alternatively, one would need to simulate $N \sim 10,000$ trajectories over the time scale of $t_D \sim 10^5$ to measure D with a 10% accuracy, corresponding to $A = 10$.

On the other hand, for the parameters used to produce the plot in Fig. 3.2 ($\sigma^2_{plateau} = 10^8, \ D = 1, \ N = 1000$) we must wait over 2.10^7 time units to reliably measure D. The time scale of 10^5 time units, see the right inset in Fig. 3.2, is way too short to reveal an increase of $\sigma_x^2(t)$. Over this time scale, the time evolution of $\sigma_x^2(t)$ may even exhibit an overall decrease, which is entirely due to the small sampling size.

Finally, for the initial temperature $T_0 = 10^4$ we have $t_D = 2.10^3$, much shorter than the time of measurement in Fig. 3.2. It is for this reason that the coordinate dispersion increases linearly with time on the linear scale (Fig. 3.2, left inset) in spite of the plateau observed on the logarithmic scale.

3.4.3 Determination of the diffusion coefficient in the plateau region

Fortunately, to accurately determine the diffusion coefficient from the simulations, it is not necessary to wait for such a long time or to simulate a huge number of trajectories. Instead,

one may adopt the following numerical procedure.

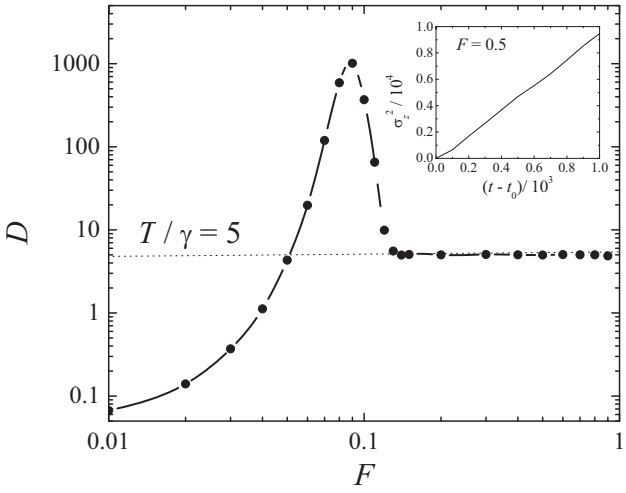

Figure 3.3 – Diffusion coefficient D vs. applied bias F for the same parameters as in Fig. 3.1. All data points were obtained from the slope of the dispersion $\sigma_z^2(t)$ line in the plateau region, see inset showing this line for $F = 0.5$. For convenience, the time is measured from the moment $t_0 = 10^4$ inside the plateau of $\sigma_x^2(t)$.

First, the system is simulated to the point t_0 when the initial transient process has decayed and the dispersion plateau has started. The time t_0 does not have to be very large; for instance, for the parameters from Fig. 3.1, it may be $t_0 = 10^4$. At the time t_0, the coordinate of the particle x_{t_0} is a random variable characterized by a very broad distribution. Hence, one needs to measure the dispersion of an auxiliary variable

$$z_t = x_t - x_{t_0} = y_t - y_{t_0} + v_\infty(t - t_0) \ ,$$
$$\sigma_z^2(t) = \langle z_t^2 \rangle - \langle z_t \rangle^2 = 2D(t - t_0) \ , \tag{3.20}$$

see the discussion above. Again, neither the simulation time nor the number of trajectories N have to be very large: as Fig. 3.3 exemplifies, a very small portion of the total duration

of the plateau phase is sufficient to get a linear increase of $\sigma_z^2(t)$ with very little fluctuations for $N = 1000$.

In this way, we were able to obtain the force-dependent diffusion coefficient of the system (3.1) with the parameters (other than force) specified in the captions to Fig. 3.1, also covering the range of forces $0.1 < F < 1$ which was unaccessible for the procedure adopted in [9]. At these forces, the diffusion coefficient is practically constant and has the value $T/\gamma = 5$, see Fig. 3.3. This value corresponds to the so-colled running state of the Brownian particle. At low forces, $F < 0.1$ in Fig. 3.3, the diffusion proceeds via thermally activated hopping over one or more barriers that separate the adjacent minima of the total potential $U(x) - Fx$; since those barriers decrease with force, $D(F)$ increases until it reaches a maximum. This maximum is due to the high frequency of switching between the running and the locked states, which leads to the fastest temporal growth of the particle coordinate dispersion in the frame of reference which moves with the average velocity of the particle.

3.5 Conclusions

The "dispersionless transport" phenomenon is actually more ubiquitous than suggested in the original paper [9]. It can be expected in any noisy system, in which there is an initial transient process leading to a broad spreading of the coordinate. After the decay of this process, a plateau in the coordinate dispersion can be expected for some time.

Even though the numerical examples discussed in this paper involve a Brownian particle with finite mass and relatively low damping, one can easily think of other possible scenarios that result in a dispersion plateau even in the overdamped limit, see Eq. (3.1) with m formally set to 0. For instance, consider the free diffusion of an overdamped Brownian particle: $\dot{x}_t = \sqrt{2T/\gamma}\xi(t)$. One may start with a high temperature $T = T_H$, and then abruptly change the temperature to a much lower value $T = T_L \ll T_H$ at some time $t_0 > 0$.

Then, for $t \gg t_0$, the dispersion will increase according to Eq. (3.5) with $D = T_L/\gamma$ and $\sigma^2_{plateau} = 2t_0 T_H/\gamma$. On the logarithmic scale, the dispersion will have a plateau of duration $t_{plateau} = t_0 T_H/T_L \gg t_0$, which can be made arbitrarily long by adjusting the ratio T_H/T_L.

Another question is, why the diffusion coefficient cannot be extracted from the dispersion vs. time plot in the plateau region. This has to do with both the large initial value of the dispersion and with the fact that averaging is performed over a finite number of stochastic trajectories. In practice, the existence of the dispersion plateau does not pose a problem in a numerical determination of the diffusion coefficient. The only modification that is required to perform this measurement is to account for the distribution of the initial position in the beginning of the plateau phase. The deviation of the coordinate from the initial position does exhibit the standard linear increase characteristic of the regular diffusive process. Because the linear increase of the dispersion within the plateau region is measurable, we believe that the term "dispersionless transport" is actually a misnomer and used it in quotation marks throughout this paper.

Acknowledgements

The authors are grateful to the Natural Sciences and Engineering Research Council of Canada (NSERC) for financial support through the Discovery Grant (2015-04486) and ACEnet for computational resources.

Bibliography

[1] A. Kaffashnia, M. Evstigneev. dispersionless transport in spite of thermal noise. *Phys.Rev. E*, **104**, 054113, (2021).

[2] L. Gammaitoni, P. Hänggi, P. Jung, and F. Marchesoni. Stochastic resonance. *Rev. Mod. Phys.*, **70**, 223, (1998).

[3] P. Reimann. Brownian motors: noisy transport far from equilibrium. *Phys. Rep.*, **361**, 57, (2002).

[4] R. Eichhorn, P. Reimann, and P. Hänggi. Brownian motion exhibiting absolute negative mobility. *Phys. Rev. Lett.*, **88**, 190601, (2002).

[5] B. Cleuren and C. van den Broeck. Brownian motion with absolute negative mobility. *Phys. Rev. E.*, **67**, 055101, (2003).

[6] A. Sarracino, F. Cecconi, A. Puglisi, and A. Vulpiani. Nonlinear response of inertial tracers in steady laminar flows: Differential and absolute negative mobility. *Phys. Rev. Lett.*, **177**, 174501, (2016).

[7] J. Cividini, D. Mukamel, and HA. Posch. Driven tracer with absolute negative mobility. *J. Phys. A: Math. Theor.*, **51**, 085001, (2018).

[8] J. Wang, G. Casati, and G. Benenti. Inverse currents in Hamiltonian coupled transport. *Phys. Rev. Lett.*, **124**, 110607, (2020).

[9] K. Lindenberg, J.M. Sancho, A.M. Lacasta, and I.M. Sokolov. Dispersionless transport in a washboard potential. *Phys. Rev. Lett.*, **98**, 020602, (2007).

[10] W.L. Reenbohn, S. Saikia, R. Roy, and M.C. Mahato. Motional dispersions and ratchet effect in inertial systems. *Pramana - J. Phys.*, **71**, 297, (2008).

[11] S. Saikia and M.C. Mahato. Dispersionless motion in a periodically rocked periodic potential. *Phys. Rev. E.*, **80**, 062102, (2009).

[12] S. Saikia and M.C. Mahato. Dispersionless motion and ratchet effect in a square-wave-driven inertial periodic potential system. *J. Phys.: Condens. Matter*, **21**, 175409, (2009).

[13] W. Guo, L.C. Du, and D.C. Mei. Anomalous diffusion and enhancement of diffusion in a vibrational motor. *J. Stat. Mech.*, P04025, (2014).

[14] M.S. Simon, J.M. Sancho, and K. Lindenberg. Transport and diffusion of underdamped Brownian particles in random potentials. *Eur. Phys. J. B.*, **87**, 201, (2014).

[15] P. Hänggi, P. Talkner, and M. Borkovec. Reaction-rate theory: fifty years after Kramers. *Rev. Mod. Phys.*, **62**, 251, (1990).

Chapter 4

Diffusion coefficient scaling of a free Brownian particle with velocity-dependent damping

In this chapter, we reproduce our third collaborative work by Mykhaylo Evstigneev and Amir Kaffashnia, as referenced in [1] with kind permission of the publishers of Physical Review E. The paper can be accessed through the DOI link: 10.1103/PhysRevE.107.064129.

4.1 Abstract

An analytical expression for the diffusion coefficient D of a free Brownian particle with velocity-dependent damping $\gamma(v)$ is derived from the Green-Kubo formula. A special case of damping that monotonically decreases with velocity is considered. At high temperature T, the diffusion coefficient is found to exhibit two scaling types: (i) for a power-law decrease of damping with the particle's kinetic energy, $\gamma(v) \propto 1/v^{2\alpha}$, it scales as $D \propto T^{\alpha+1}$; (ii) for a Gaussian function $\gamma(v)$ it diverges at temperatures above a critical value T_c and behaves

as $D \propto 1/\sqrt{T_c - T}$ at $T < T_c$. In case (ii) at $T > T_c$ the particle trajectory contains long flight events, which are not observed at $T < T_c$ and in case (i) at all temperatures.

4.2 Introduction

Sutherland-Einstein-Smoluchowski formula expresses the diffusion coefficient of a free particle as a ratio of thermal energy T to the damping coefficient γ [2,3]:

$$D = T/\gamma \ . \tag{4.1}$$

Its breakdown in various systems has been drawing attention recently [4–10].

A standard way of deriving Eq. (4.1) relies on the Langevin equation of motion, $m\dot{v} = f_{diss} + f_{noise}$, in which the dissipative force on the Brownian particle of mass m, $f_{diss} = -\gamma v$, is proportional to its velocity v [2]. Hence, the simplest model in which Eq. (4.1) does not hold, is that of a free Brownian particle with velocity-dependent damping. Such model is more realistic than the standard Langevin equation with constant γ, because in real liquids and gases, the simple proportionality between dissipative force and velocity is an approximation valid in the limit of small Reynolds numbers and not too high velocities.

The Langevin equation with velocity-dependent damping, $\gamma = \gamma(v)$, can be derived from first principles, as done by Mori using projection operator technique [11]. In Ref. [12], this derivation was based on master equation, from which damping was expressed in terms of the transition probability between two momentum states of the particle. At a phenomenological level, the function $\gamma(v)$ is chosen based on the physical properties of the system under consideration. Various functional forms for the velocity-dependent damping $\gamma(v)$ appear in the literature. Marchesoni [13] chose it based on Sutherland's formula [3] for the temperature-dependent viscosity of a liquid. Braun et al [14–16] studied diffusion of adatoms on a solid surface and related $\gamma(v)$) to the density of surface phonon states.

Somewhat outside of the scope of this paper, a Reyleigh-Helmholtz and other expressions allowing for $\gamma(v)$ to become negative are used in the models of active Brownian motion [17–19].

The other force on a free Brownian particle in the Langevin equation is thermal noise f_{noise} due to thermal motion of the environment atoms. If this chaotic motion proceeds much faster than the dynamics of the Brownian particle, the thermal noise can be approximated as Gaussian and white. For velocity-independent γ, noise intensity is given by the fluctuation-dissipation theorem of the second kind [2] as $2\gamma T$. If $\gamma(v)$ is velocity-dependent, noise intensity also becomes a function of velocity, as derived by Braun [14, 15] and by Trigger *et al.* [20]; see also the next section.

The relation (4.1) has been generalized in several ways. Lifson and Jackson derived an analytical expression for the diffusion coefficient of an overdamped particle in a periodic potential [21]; this expression was further developed by Reimann *et al.* [22] to include a constant tilting force. With respect to diffusion with velocity-dependent damping, Trigger *et al.* found an analytic expression for the diffusion coefficient [20] by considering relaxation of the particle probability distribution from a small spatial inhomogeneity to equilibrium.

Here, we derive the diffusion coefficient based on a different approach than in Ref. [20], namely, by applying the Green-Kubo formula to the Langevin equation. We consider a broad class of functions $\gamma(v)$ that monotonically decrease with v^2. We show that if damping decreases at high velocities as $\gamma(v) \propto 1/v^{2\alpha}$, the diffusion coefficient indeed scales as $D(T) \propto T^{\alpha+1}$, as conjectured earlier in [23, 24]. Furthermore, we find that if damping decreases faster than any power of the velocity, the diffusion coefficient diverges above a certain critical temperature T_c. Specifically, for a Gaussian Ansatz for $\gamma(v)$, the diffusion coefficient turns out to scale as $D(T) \propto 1/\sqrt{T_c - T}$. We confirm these results by numerical simulations.

4.3 Langevin and Fokker-Planck equation

In view of isotropy and homogeneity of space, we can limit ourselves to just one spacial coordinate x. Langevin equation of a free particle with velocity-dependent damping reads [11, 13–15]

$$m\dot{v} = -\gamma(v)v + g(v)\xi(t) \ , \quad \dot{x} = v \ ,$$
$$\langle \xi(t) \rangle = 0 \ , \quad \langle \xi(t)\xi(t') \rangle = \delta(t-t') \ . \tag{4.2}$$

The noise $\xi(t)$ is unbiased, Gaussian, and white. Due to space inversion symmetry, both $\gamma(v)$ and $g(v)$ are even functions of velocity v.

To relate the noise-coupling function $g(v)$ to the damping coefficient $\gamma(v)$, and also to introduce the formulae to be used later on, we briefly outline the derivation from [15] and write down the Fokker-Planck equation for the time-dependent velocity probability density $W(v,t)$ [2],

$$\frac{\partial W(v,t)}{\partial t} = \hat{\mathcal{L}}(v)W = \frac{1}{m}\frac{\partial}{\partial v}\left[\frac{g^2(v)}{2m}\frac{\partial W}{\partial v} + \left(\gamma(v)v + \frac{1}{2m}g(v)\frac{dg(v)}{dv}\right)W\right] \ , \tag{4.3}$$

in which the multiplicative noise is interpreted in the Stratonovich sense. In equilibrium, the velocity probability distribution is Maxwellian,

$$W_{eq} = \sqrt{m/(2\pi T)}e^{-mv^2/(2T)} \ , \tag{4.4}$$

and the probability current in the velocity space, proportional to the expression in the square brackets of Eq. (4.3), vanishes. This results in a differential equation for $g^2(v)$ [14, 15, 20] ,

$$\gamma(v)v + \frac{1}{4m}\frac{dg^2(v)}{dv} = \frac{g^2(v)v}{2T} \ , \tag{4.5}$$

whose solution is

$$g^2(v) = 2me^{mv^2/T}\int_{v^2}^{\infty} dy\gamma(\sqrt{y})e^{-my/T} \ . \tag{4.6}$$

4.4 Diffusion coefficient

4.4.1 Derivation from the Green-Kubo formula

The diffusion coefficient is given by the equivalent expressions

$$D = \lim_{t\to\infty} \frac{\langle x^2(t)\rangle}{2t} = \int_0^\infty dt\, \langle v(t)v(0)\rangle = \langle X(v)v\rangle \ , \tag{4.7}$$

where $X(v) = \int_0^\infty dt\, \langle v(t)\rangle_{v(0)=v}$ is the mean displacement of the particle for a fixed initial velocity $v(0) = v$. In the last formulation, averaging is performed over the equilibrium distribution (4.4) of initial velocities. The expression of D as an integral over the velocity autocorrelation function is known as Green-Kubo formula.

Let us denote the transition probability density in the velocity space by $P(v', t|v)$. It obeys the Fokker-Planck equation (4.3), $\partial P/\partial t = \hat{\mathcal{L}}(v')P$, with the initial condition $P(v', 0|v) = \delta(v' - v)$; the formal solution of this equation is $P(v', t|v) = e^{\hat{\mathcal{L}}(v')t}\delta(v' - v)$. Given the sharp initial velocity value v, the average velocity at time t is

$$\langle v(t)\rangle = \int_{-\infty}^{\infty} dv' v' P(v', t|v) \ . \tag{4.8}$$

Hence,

$$\begin{aligned} X(v) \quad &= \textstyle\int_0^\infty dt \int_{-\infty}^{\infty} dv' v' e^{\hat{\mathcal{L}}(v')t}\delta(v' - v) \\ &= \textstyle\int_0^\infty dt \int_{-\infty}^{\infty} dv' \delta(v' - v) e^{\hat{\mathcal{L}}^\dagger(v')t} v' \\ &= \textstyle\int_0^\infty dt e^{\hat{\mathcal{L}}^\dagger(v)t} v = -[\hat{\mathcal{L}}^\dagger(v)]^{-1} v \ . \end{aligned} \tag{4.9}$$

In the second line we used the adjoint Fokker-Planck operator $\hat{\mathcal{L}}^\dagger$, and in the third line we first integrated over v' and then over t.

Incorporating the relation (4.5) in the definition (4.3), we write the Fokker-Planck operator in a more compact form:

$$\hat{\mathcal{L}}(v) = \frac{1}{2mT}\frac{d}{dv}\left[g^2(v)\left(\frac{T}{m}\frac{d}{dv} + v\right)\right] \ . \tag{4.10}$$

After taking its conjugate, we obtain the differential equation for the average displacement by acting with $\hat{\mathcal{L}}^\dagger$ on both sides of Eq. (4.9):

$$\hat{\mathcal{L}}^\dagger(v)X(v) \equiv \frac{1}{2mT}\left(\frac{T}{m}\frac{d}{dv} - v\right) g^2(v)\frac{dX(v)}{dv} = -v \ . \tag{4.11}$$

It must be supplemented by two boundary conditions. The first one is obvious: since the displacement is an odd function of the initial velocity, $X(-v) = -X(v)$, its value at zero initial velocity is $X(0) = 0$.

The second boundary condition is formulated by considering the limiting case of a large positive initial velocity $v \gg \sqrt{T/m}$. If it is further increased by a small amount dv, the average distance should increase by

$$dX = v d\mathcal{T}(v) \ , \tag{4.12}$$

where $\mathcal{T}(v)$ is the mean time after which the particle's velocity first reaches the value 0, and $d\mathcal{T}(v)$ is the mean time for velocity to decrease from $v + dv$ to v. The relation (4.12) is valid only in the high-velocity limit, in which the "sliding down" in the velocity space from $v + dv$ to v is quasideterministic, implying that the dispersion of the respective deceleration time around $d\mathcal{T}$ is negligible.

The mean first passage time $\mathcal{T}(v)$ is found by solving the equation $\hat{\mathcal{L}}^\dagger(v)\mathcal{T}(v) = -1$ with an absorbing boundary condition at $v = 0$ and a reflecting boundary condition at $v = \infty$, see [25]. Its velocity derivative is

$$\frac{d\mathcal{T}(v)}{dv} = 2m^2 \ \frac{e^{mv^2/(2T)}}{g^2(v)} \int_v^\infty dv_1 e^{mv_1^2/(2T)} \ , \tag{4.13}$$

and $\mathcal{T}(v)$ is obtained by integrating this expression from 0 to v. At high velocities the integral in Eq. (4.13) behaves asymptotically as $\frac{T}{mv}e^{-mv^2/(2T)}$, and thus $d\mathcal{T}/dv \to 2mT/(vg^2(v))$; it then follows from Eq. (4.12) that at high velocities we should have $dX/dv \to 2mT/g^2(v)$.

The solution of Eq. (4.11) consistent with the boundary conditions is

$$X(v) = 2mT \int_0^v \frac{dv'}{g^2(v')} \ . \tag{4.14}$$

Substitution of Eq. (4.14) into Eq. (4.7) gives the diffusion coefficient

$$D = 2mT \int_{-\infty}^{\infty} dv \ vW_{eq}(v) \ \int_0^v \frac{dv'}{g^2(v')} \tag{4.15}$$

with $g^2(v)$ given by Eq. (4.6).

4.4.2 Damping coefficient ansatz

We will apply Eq. (4.15) to study the scaling of the diffusion coefficient in the interesting case when damping $\gamma(v)$ is a decreasing function of the particle's kinetic energy. This is common in the situations in which the environment does not efficiently absorb the particle's energy at high velocities due to the finite reaction time of the environment atoms [14, 15, 23, 24] . We parameterize the velocity-dependent damping coefficient by its value $\gamma_0 = \gamma(0)$ in the low-velocity limit, the characteristic velocity u, at which damping decreases by a specified amount, and an exponent $\alpha > 0$ which controls the manner in which $\gamma(v)$ decreases from the value γ_0 to zero at $v \to \infty$:

$$\gamma(v) = \frac{\gamma_0}{(1 + \frac{v^2}{\alpha u^2})^\alpha} \ . \tag{4.16}$$

The noise coupling function (4.6) is

$$g^2(v) = 2\alpha\gamma_0 mu^2 \frac{F_\alpha(m(v^2 + \alpha u^2)/T)}{[1 + v^2/(\alpha u^2)]^{\alpha-1}} \ , \tag{4.17}$$

where

$$F_\alpha(x) = \int_0^\infty dt \frac{e^{-xt}}{(t+1)^\alpha} \tag{4.18}$$

is closely related to the incomplete gamma function $\Gamma(s,x) = \int_x^\infty dt \ t^{s-1}e^{-t}$ by $F_\alpha(x) = e^\alpha x^{\alpha-1}\Gamma(1-\alpha, x)$.

The average displacement (4.14) and the diffusion coefficient (4.15) expressions are obtained by a straightforward change of integration variables:

$$\begin{aligned} X(v) &= \tfrac{T^{3/2}}{\alpha\gamma_0\sqrt{mu^2}} I(v\sqrt{m/T}) \ , \\ D &= \sqrt{\tfrac{2}{\pi}} \tfrac{T^2}{\alpha\gamma_0 mu^2} \int_0^\infty dy e^{-y} I(\sqrt{2y}) \ , \\ I(y) &= \int_0^y dz \tfrac{[1+z^2T/(\alpha mu^2)]^{\alpha-1}}{F_\alpha(z^2+\alpha mu^2/T)} \ . \end{aligned} \tag{4.19}$$

An interesting special case is the Gaussian limit $\alpha \to \infty$, in which

$$\gamma(v) = \gamma_0 e^{-v^2/u^2} \ , \ g^2(v) = \frac{2\gamma(v)T}{1+\frac{T}{mu^2}} \ . \tag{4.20}$$

The average displacement (4.14) is then given by

$$X(v) = u\tau \frac{\sqrt{\pi}}{2} \mathrm{erfi}(v/u) \ , \ \tau = \frac{m}{\gamma_0}\left(1+\frac{T}{mu^2}\right) \tag{4.21}$$

where $\mathrm{erfi}(y) = \frac{2}{\sqrt{\pi}} \int_0^\infty dz e^{z^2}$ is imaginary error function. The diffusion coefficient is

$$D = u\tau\sqrt{\frac{T}{2m}} \int_0^\infty dy e^{-y} \mathrm{erfi}\left(u^{-1}\sqrt{\frac{2Ty}{m}}\right) \ . \tag{4.22}$$

4.5 Temperature scaling of the diffusion coefficient

4.5.1 Simulation details

The tricky part in simulating Eq. (4.2) has to do with the multiplicative noise, which results in the Itô-Stratonovich ambiguity of the time discretization procedure. Although this ambiguity can be resolved [26,27], we chose to avoid it completely and to work with an auxiliary variable

$$\phi(v) := \int_0^v dv' \frac{g(0)}{g(v')} \ , \ \phi_t \equiv \phi(v_t) \ , \tag{4.23}$$

whose dynamics is governed by a Langevin equation with additive noise

$$m\dot{\phi}_t = -\frac{g(0)}{g(v(\phi_t))}\gamma(v(\phi_t))v(\phi_t) + g(0)\xi(t) \ , \tag{4.24}$$

as can be obtained by multiplying both sides of Eq. (4.2) with $g(0) = g(v)$. The function $v(\phi)$ is obtained by inverting Eq. (4.23).

To save computational effort, the functions $\phi(v)$ and $g(v)$ were tabulated with the velocity v assuming discrete values from -10$\sqrt{T/m}$ to 10$\sqrt{T/m}$ in steps of 0.01$\sqrt{T/m}$. These tabulated values were used by the code to quickly find the velocity v and the "force" $F(\phi) = -g(0)\gamma(v(\phi))v(\phi)/g(v(\phi))$ corresponding to a given ϕ by performing cubic interpolation based on the four support points closest to the current value of ϕ. The stochastic differential equation (4.24) was discretized according to the Euler scheme, i.e. $m(\phi_{n+1} - \phi_n)/\Delta t = F(\phi_n) + g(0)\xi_n/\sqrt{\Delta t}$, where ξ_n are unbiased Gaussian random numbers with unit variance, $\langle \xi_n \xi_{n'} \rangle = \delta_{nn'}$, and ϕ_n is the value of ϕ on the n^{th} time step.

In the simulations, we set without loss of generality the parameters$m$, u, and γ_0 to 1; this uniquely fixes the units of mass, time, and length to m, m/γ_0, and mu/γ_0, respectively.

The diffusion coefficient D was found as a long-time limit of the time-dependent counterpart

$$D(t) = \frac{\left\langle [x(t) - x(0)]^2 \right\rangle}{2t} \ . \tag{4.25}$$

After each measurement of the displacement $x(t) - x(0)$, the particle velocity was reset to a random value according to the Maxwellian distribution (4.4); this ensured that successive displacement measurements were independent of each other.

4.5.2 Particle trajectories

Before we go on to the discussion of the diffusion coefficient, it is instructive to consider several representative trajectories at two extreme values of the parameter α and at different temperatures T. In Fig. 4.1 we compare the representative trajectories of the particle obtained for the Lorentzian model, Eqs. (4.16), (4.17) with $\alpha = 1$, and Gaussian model, Eq. (4.20). In the Lorentzian case the trajectories do not differ qualitatively at all temperatures.

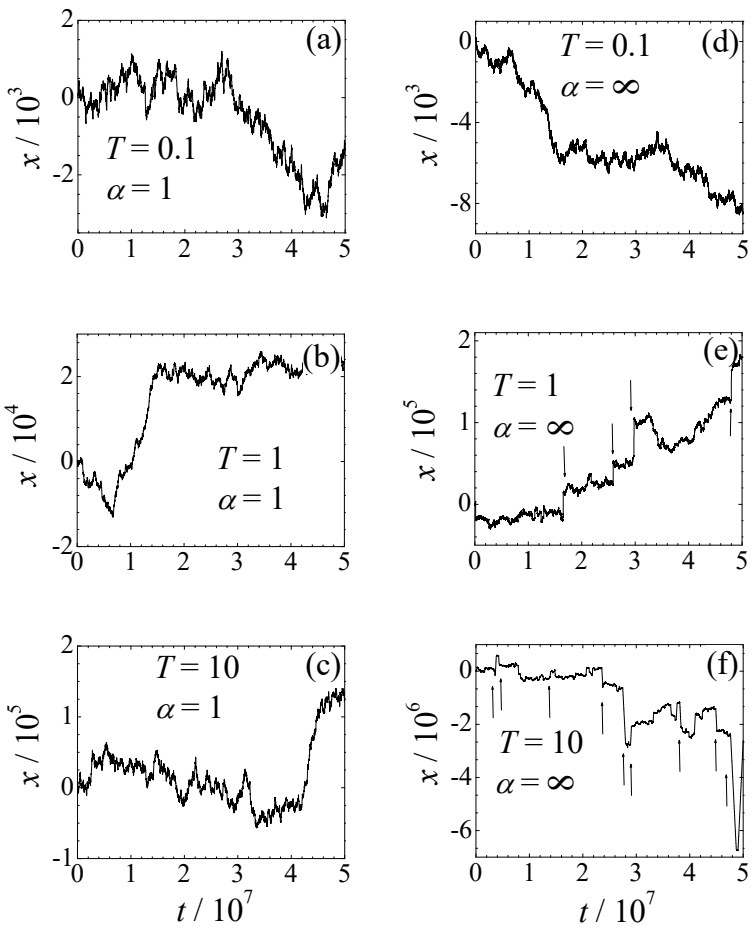

Figure 4.1 – Sample trajectories (4.2) obtained numerically within (a)-(c) Lorentzian damping model, Eq. (4.16) with $\alpha = 1$, and (d)-(f) Gaussian model (4.20). The long flight events in graphs (e) and (f) are indicated with arrows.

They represent erratic motion, whose scale grows with temperature $T = 0.1, 1$, and 10 in panels (a), (b), and (c), respectively. We observed qualitatively similar trajectories for all other finite values of the exponent α between 1 and 10 that we tested.

Turning to the Gaussian model, Fig. 4.1(d), (e), and (f), we see that at the smallest temperature $T = 0.1$, the trajectory looks similar to the one in the Lorentzian model, cf.

Fig. 4.1(a) and (d). But increasing the temperature leads to the appearance of a new feature in the particle's dynamics, namely, its regular diffusion becomes interrupted by long flight events, which are marked with arrows in Fig. 4.1(e) and (f).

Long jumps over more than one lattice spacing have been observed both experimentally and in molecular dynamics simulations of surface diffusion of individual atoms [28–32], molecules [33,34], and nanoclusters [35–37]. Stochastic simulations of adatom diffusion relying on the Langevin equation with velocity-independent damping [38] yield a much weaker temperature dependence of the frequency of long jump events than observed xperimentally [28, 29]. Consequently, Braun, Peyrard, and Ferrando [14–16] extended the Langevin model by including velocity dependence of the damping coefficient.

While long jumps in the surface diffusion literature [28–37] are defined as transitions by more than one lattice constant, the diffusion of a free Brownian particle does not have this built-in length scale. Hence, we define long flight events in a different manner by two properties:

(i) The velocity does not change sign during the event duration Δt;

(ii) The distance Δx travelled by the particle during the event exceeds the distance over which the particle would typically diffuse given the same amount of time,

$$\Delta x^2 > 2D(\Delta t)\Delta t \ , \tag{4.26}$$

where the time-dependent diffusion coefficient is defined by Eq. (4.25).

If surface diffusion proceeds predominantly via single jumps, then transitions over more than one lattice constant are covered by this definition of long flights.

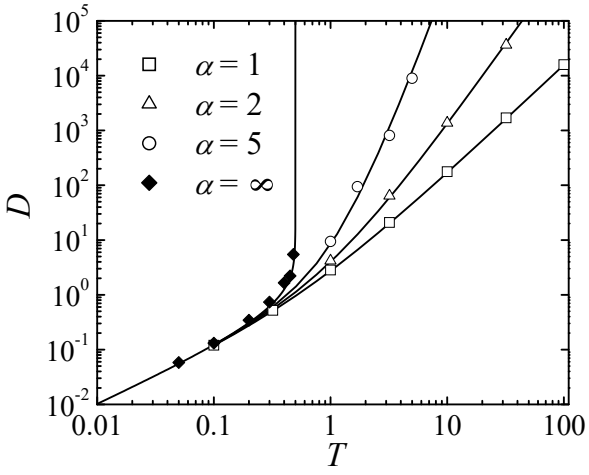

Figure 4.2 – Diffusion coefficient vs. temperature for the model (4.2) with the damping coefficient given by Eq. (4.16) at $\alpha = 1$, 2, 5, and for the Gaussian model (4.20) corresponding to the limit $\alpha \to \infty$. Symbols: simulation results; lines: analytical formula (4.19) (for finite α) and (4.22) (for $\alpha \to \infty$).

4.5.3 Diffusion coefficient vs. temperature

Fig. 4.2 shows the theoretical curves (4.19) and (4.22) (lines) and simulation results (symbols) for the temperature-dependent diffusion coefficient. At low temperatures, both models predict the same linear increase $D = T/\gamma_0$ according to the standard relation (4.1). For finite values of α, the high-temperature asymptotic behavior of the diffusion coefficient is obtained from Eq. (4.19):

$$D \propto T^{\alpha+1} \; for \; \alpha < \infty \; , \tag{4.27}$$

because the dominant contribution to $I(y)$ is proportional to $T^{\alpha-1}$. Such scaling of the diffusion coefficient with temperature was reported by Silvius et al for a special case $\gamma(v) \propto 1/v^3$, i.e. $\alpha = 3/2$, resulting in the temperature scaling $D(T) \propto T^{5/2}$ [23]. A straightforward generalization of their argument indeed gives the relation (4.27) for arbitrary α, see [24]. Even though the particle considered in Refs. [23,24] performed thermal motion in a periodic

structure, this scaling was obtained in the high-temperature asymptotic limit, in which the effect of the periodic structure should be negligible, i.e. the particle could be treated as approximately free.

Granted, the scaling behaviour (4.27) is not very surprising and can be understood within Einstein's relation (4.1) by approximating $D \approx T/\gamma(v_{th})$, where $v_{th} = \sqrt{T/m}$ is thermal velocity. But this sort of argument does not apply in the Gaussian limit (4.22). At large values of its argument $y \gg 1$, the imaginary error function behaves as $\mathrm{erfi}(y) \propto \frac{e^{y^2}}{y\sqrt{\pi}}$. Then, as can be seen from Eq. (4.21), the mean displacement depends on the initial velocity as $X(v) \propto v^{-1}e^{v^2/u^2}$ at $|v| \gg u$. With respect to the diffusion coefficient, the integral diverges when the temperature exceeds the critical value:

$$D \to \infty \;\; at \;\; T \geq T_c = \frac{mu^2}{2} \; . \tag{4.28}$$

To derive the asymptotic behavior of the function $D(T)$ slightly below the critical temperature, we split the integral (4.22) into two parts: one from 0 to a large but finite number a, and the other from a to ∞. The former contribution remains finite, while the latter diverges as $T \to T_c$. With the help of the above asymptotic expression for the imaginary error function, we obtain the divergent part of the diffusion coefficient:

$$D \propto \frac{\tau u^2}{2\sqrt{\pi}} \int_a^\infty dy \frac{e^{-y(1-T/T_c)}}{\sqrt{y}} \propto \frac{\tau u^2}{2\sqrt{1-\frac{T}{T_c}}} \; . \tag{4.29}$$

In the second step, we changed the integration variable to $y' = y(1 - T/T_c)$ and evaluated the integral in the limit $T/T_c \to 1^-$ using the formula $\int_0^\infty dy' e^{-y'}/\sqrt{y'} = \sqrt{\pi}$.

At $T > T_c$, the diffusion coefficient (4.22) is infinite, which is manifested in unlimited increase of the time-dependent diffusion coefficient (4.25) observed in the simulations. In this regime, the particle undergoes superdiffusion, see, e.g. [39] and references therein. The time-dependent diffusion coefficient at $T > T_c$ increases as $D(t) \propto t^\lambda$ with $0 < \lambda < 1$. As our simulations revealed, the exponent λ is temperature-dependent; it grows from the value

close to 0 at $T = T_c$ and saturates at T above several T_c at $\lambda = 1$, which corresponds to ballistic Brownian motion.

4.6 Conclusion

In view of its simplicity, Langevin equation with velocity-dependent damping $\gamma(v)$ is a useful tool in describing diffusion of small objects, from atoms to nanoparticles. Their velocity-dependent damping $\gamma(v)$ and diffusion coefficient D can be measured independently of each other. Hence, the relation (4.15) between them is amenable to direct verification both in an experiment and in a molecular dynamics simulation.

In this paper we derived this relation from the Green-Kubo formula and applied it to study the temperature dependence of the diffusion coefficient for the velocity-dependent damping (4.16) that monotonically decreases with the particle's velocity. At low temperatures, diffusion coefficient grows linearly with temperature, $D = T/\gamma(0)$, for all values of the parameter α that controls the manner in which the function $\gamma(v)$ goes to zero with v. The high-temperature scaling behaviour of $D(T)$ is drastically different for a power-law and exponential decrease of damping with the particle's kinetic energy. Namely, in the former case, the diffusion coefficient likewise exhibits a power-law temperature dependence, while in the latter case it diverges at some critical temperature.

The presence of long flights, as defined in the end of Section 4.5.2, is correlated with this difference, as long flight events are observed only for the Gaussian damping model above the critical temperature. The Brownian particle in this regime undergoes superdiffusive dynamics. A more detailed study of this interesting regime will be performed in the future.

Acknowledgments

We thank the Natural Sciences and Engineering Research Council of Canada (NSERC) for financial support through the Discovery Grant 2015-04486 and ACEnet for computational resources.

Bibliography

[1] M. Evstigneev and A. Kaffashnia. Diffusion coefficient scaling of a free Brownian particle with velocity-dependent damping. *Phys. Rev. E*, **107**, 064129, (2023).

[2] H. Risken. *Fokker-Planck Equation* (Springer, Berlin, Heidelberg, 1996).

[3] S. Chapman and T.G. Cowling. *The Mathematical Theory of Non-Uniform Gases* (Cambridge University Press, Cambridge, 1991).

[4] P. Charbonneau, Y. Jin, G. Parisi, and F. Zamponie. Hopping and the Stokes–Einstein relation breakdown in simple glass formers. *Proc. Natl. Acad. Sci. U.S.A.*, **111**, 15025, (2014).

[5] N. Ohtori, Sh. Miyamoto, and Y. Ishii. Breakdown of the Stokes-Einstein relation in pure Lennard-Jones fluids: From gas to liquid via supercritical states. *Phys. Rev. E*, **95**, 052122, (2017).

[6] Sh. Wei, Z. Evenson, M. Stolpe, P. Lucas, and C.A. Angell. Breakdown of the Stokes-Einstein relation above the melting temperature in a liquid phase-change material. *Sci. Adv.*, **4**, eaat8632, (2018).

[7] L. Costigliola, D.M. Heyes, Th.B. Schroder,1 and J.C. Dyre. Revisiting the Stokes-Einstein relation without a hydrodynamic diameter. *J. Chem. Phys.*, **150**, 021101, (2019).

[8] V. Dubey, Sh. Erimban, S. Indra, and S. Daschakraborty. Understanding the origin of the breakdown of the Stokes–Einstein relation in supercooled water at different temperature–pressure conditions. *J. Phys. Chem. B*, **123**, 10089, (2019).

[9] V. Dubey and S. Daschakraborty. Breakdown of the Stokes–Einstein Relation in Supercooled Water/Methanol Binary Mixtures: Explanation Using the Translational Jump-Diffusion Approach. *J. Phys. Chem. B*, **124**, 10398, (2020).

[10] Sh. Kumar, S. Sarkar and B. Bagchi. Microscopic origin of breakdown of Stokes–Einstein relation in binary mixtures: Inherent structure analysis. *J. Chem. Phys.*, **152**, 164507, (2020).

[11] H. Mori, H. Fujisaka, and H. Shigematsu. A new expansion of the master equation. *Prog. Theor. Phys.*, **51**, 109, (1974).

[12] S.A. Trigger. Fokker-Planck equation for Boltzmann-type and active particles: Transfer probability approach. *Phys. Rev. E*, **67**, 046403, (2003).

[13] F. Marchesoni. A nonlinear Langevin equation for fluid relaxation. *Prog. Theor. Phys.*, **74**, 1339, (1985).

[14] O. Braun and M. Peyrard. Friction in a solid lubricant film. *Phys. Rev. E*, **63**, 046110, (2001).

[15] O. Braun and R. Ferrando. Role of long jumps in surface diffusion. *Phys. Rev. E*, **65**, 061107, (2002).

[16] O. Braun. Phenomenological theory of kinetic friction for the solid lubricant film. *Phys. Scr.*, **78**, 015802, (2008).

[17] W. Ebeling, J. Dunkel, U. Erdmann, and S. Trigger. Klimontovich's contributions to the kinetic theory of nonlinear Brownian motion and new developments. *J. Phys.: Conf. Ser.*, **11**, 89, (2005).

[18] P. Romanczuk, M. Bär, W. Ebeling, B. Lindner, and L. Schimansky-Geier. Active Brownian particles: From individual to collective stochastic dynamics. *Eur. Phys. J. Special Topics*, **202**, 1, (2012).

[19] A. Yazdi and M. Sperl. Glassy dynamics of Brownian particles with velocity-dependent friction. *Phys. Rev. E*, **94**, 032602, (2016).

[20] S.A. Trigger, G.J.F. van Heijst, and P.P.J.M. Schram. Velocity-dependent friction and diffusion for grains in neutral gases, dusty plasmas and active systems. *Physica A*, **347**, 77, (2005).

[21] S. Lifson and J.L. Jackson. On the self-diffusion of ions in a polyelectrolyte solution. *J. Chem. Phys.*, **36**, 2410, (1962).

[22] P. Reimann, C. Van den Broeck, H. Linke, P. Hänggi, J.M. Rubi, and A. Pérez-Madrid. Giant acceleration of free diffusion by use of tilted periodic potentials. *Phys. Rev. Lett.*, **87**, 010602, (2001); Diffusion in tilted periodic potentials: Enhancement, universality, and scaling. *Phys. Rev. E*, **65**, 031104, (2002).

[23] A. Silvius, P.E. Parris, and S De Biévre. Adiabatic-nonadiabatic transition in the diffusive Hamiltonian dynamics of a classical Holstein polaron. *Phys. Rev. E*, **73**, 014304, (2006).

[24] A. Kaffashnia and M. Evstigneev. Scaling and universality in Brownian motion on a stochastic harmonic oscillator chain. *Phys. Rev. E*, **105**, 064134, (2022).

[25] P. Hänggi, P. Talkner, and M. Borkovec. Reaction-rate theory: fifty years after Kramers. *Rev. Mod. Phys.*, **62**, 251, (1990).

[26] P. Arnold. Langevin equations with multiplicative noise: resolution of time discretization ambiguities for equilibrium systems. *Phys. Rev. E*, **61**, 6091, (2000).

[27] A.W.C. Lau and T.C. Lubensky. State-dependent diffusion: Thermodynamic consistency and its path integral formulation. *Phys. Rev. E*, **76**, 011123, (2007).

[28] D.C. Senft and G. Ehrlich. Long jumps in surface diffusion: one-dimensional migration of isolated adatoms. *Phys. Rev. Lett.*, **74**, 294, (1995).

[29] D.C. Senft. Atomic jump lengths in surface diffusion: experiment and theory. *Appl. Surf. Sci.*, **94/95**, 231, (1996).

[30] T.R. Linderoth, S. Horch, E. Lægsgaard, I. Stensgaard, and F. Besenbacher. Surface diffusion of Pt on Pt (110): Arrhenius behavior of long jumps. *Phys. Rev. Lett.*, **78**, 4978, (1997).

[31] F. Montalenti and R. Ferrando. Jumps and concerted moves in Cu, Ag, and Au (110) adatom self-diffusion. *Phys. Rev. B*, **59**, 5881, (1999).

[32] G. Antczak and G. Ehrlich. Long jumps in diffusion of iridium on W (110). *Phys. Rev. B*, **71**, 115422, (2005).

[33] K.D. Dobbs and D.J. Doren. Dynamics of molecular surface diffusion: Origins and consequences of long jumps. *J. Chem. Phys.*, **97**, 3722, (1992).

[34] G. Langewisch, J. Falter, A. Schirmeisen, and H. Fuchs. Long jumps of an organic molecule induced by atomic force microscopy manipulation. *Adv. Mater. Interfaces*, **1**, 1300013, (2014).

[35] S.C. Wang and G. Ehrlich. Diffusion of large surface clusters: direct observations on Ir (111). *Phys. Rev. Lett.*, **79**, 4234, (1997).

[36] W.D. Luedtke and U. Landman. Slip diffusion and Levy flights of an adsorbed gold nanocluster. *Phys. Rev. Lett.*, **82**, 3835, (1999).

[37] R. Guerra, U. Tartaglino, A. Vanossi, and E. Tosatti. Ballistic nanofriction. *Nature Mater.*, **9**, 634, (2010).

[38] R. Ferrando, R. Spadacini, and G.E. Tommei. Kramers problem in periodic potentials: Jump rate and jump lengths. *Phys. Rev. E*, **48**, 2437, (1993).

[39] A.S. Bodrova, A.V. Chechkin, A.G. Cherstvy, H. Safdari, I.M. Sokolov, and R. Metzler. Underdamped scaled Brownian motion:(non-) existence of the overdamped limit in anomalous diffusion. *Sci. Rep.*, **6**, 30520, (2016).

Chapter 5

Summary and Future Work

5.1 Summary

This thesis focuses on the study of Brownian motion in three 1D models: (i) a BP diffusing on a stochastic harmonic oscillator chain (SHOC), (ii) Brownian motion in a tilted periodic potential, which we call it the "standard model" henceforth, and (iii) free Brownian motion with velocity-dependent damping. The simplicity of the 1D models allows for a detailed understanding of the complex behavior of the BP and the underlying physics governing various physical systems, including polymer physics, condensed matter physics, and statistical mechanics. This study involves theoretical analysis, computer simulations, and numerical calculations to investigate the statistical and dynamical properties of Brownian motion in each of these models. The results obtained from this study are expected to contribute to the existing knowledge of Brownian motion and its applications in different areas of physics.

The three models of 1D Brownian motion studied in this thesis exhibit several distinguishing features. Firstly, the BP/SHOC model features noise and dissipation that result from the interaction between the BP and the same objects that generate the periodic potential. In contrast, the "standard model" has a periodic potential originating from a different

source than the dissipative and random forces. The model with velocity-dependent damping, on the other hand, does not experience any external potential. Secondly, the damping coefficient of the dissipative force in the BP/SHOC and standard models is independent of velocity, whereas in the velocity-dependent damping model, as the name suggests, it is velocity-dependent. Thirdly, the dissipative force in the standard model is proportional to the particle velocity, while in the BP/SHOC and velocity-dependent damping models, the dissipative force at high temperatures is inversely proportional to the particle velocity.

The examined models in this thesis capture distinct physical systems due to the dissimilarities highlighted. Specifically, the BP/SHOC model appears more appropriate for the representation of the transport of individual atoms through a narrow channel, such as a carbon nanotube. Conversely, the standard diffusion model can depict, for example, the movement of a colloidal particle in a liquid through a 1D periodic potential, e.g., created by a laser. Moreover, the velocity-dependent damping model, which features a more realistic damping coefficient compared to the constant damping coefficient, is better suited for the analysis of real gases and liquids with high velocities.

Originally, the 1D Brownian motion of a particle along a SHOC has been used to investigate the limitations of the Langevin-type description, and it has been turned out that the Langevin equation (LE) can give quantitatively and even qualitatively wrong results at high temperatures, strong coupling between the chain oscillators, or in the presence of an external force on the BP [1]. At the same time, the BP/SHOC model may serve as an ideal testing ground for other approximation schemes aimed at replacing the full-scale MD simulations of a system with a stochastic description. In our first work, our initial motivation was twofold: first, to develop a method that would address the limitations of the LE. Second, we sought to explore the breakdown of the Einsteinian diffusion scaling in this simple model. To this end, we introduced moving stochastic boundary conditions

(MSBC) on a 1D harmonic oscillator chain. We described in this work the basic framework of the MSBC for the truncated finite chain of oscillators which replaces the full infinite chain with the dissipative and random forces acting on its first and last oscillators characterized by renormalized properties. Those forces mimic the effect of the rest of the chain on the boundary oscillators. In this method, a great deal of computational effort is saved by simulating only a small part of the oscillators which are in the immediate vicinity of the BP. In addition, we introduced an optimal way to calculate the long-time diffusion coefficient D.

Alongside the new methodology, our investigations revealed the emergence of Lévy flights as long flight events at high temperatures, characterized by a power law relationship between the diffusion coefficient (D) and temperature (T) as $D \propto T^{2+\alpha}$ (Fig. 2.2). This is different from the Einstein's relation with linear relationship between D and T. Two universal scaling laws are observed in the relationship between the average time of flight $\bar{t}_f$ and the flight length l, and for the flight length probability distribution w_l, within our study. Specifically, our results demonstrate a power-law relationship, $\bar{t}_f \propto l^{2/3}$, as presented in Fig. 2.3 (b). Additionally, we observe that the probability distribution of flight lengths exhibits a decay proportional to $1/l^{\beta}$, with an exponent of $\beta = 4/3$, as depicted in Fig. 2.5. A simple theory is also proposed that explains most of these power laws. For the $T > T_{max}$ (with $T_{max} = 50$ for the weak-coupling and $T_{max} = 200$ for the strong-coupling case), determination of the diffusion coefficient scaling with temperature is practically difficult, because eventually the particle enters a "dispersionless" or non-dispersive phase, in which it moves at a constant velocity and practically does not deposit its energy into the chain. Since the time necessary for the BP to interact with the SHOC is much longer than a reasonable computation time, reliable determination of the average time of flight, flight length and the diffusion coefficient become impossible.

In our second work, we investigated the phenomenon of "dispersionless transport" of a

BP in a tilted periodic potential which is originally reported by Lindenberg et al [2]. In this phenomenon the dispersion of the BP enters a plateau regime and appears to stay constant over a very broad time interval. Hence, the measurement of the diffusion coefficient requires prohibitively long time. We showed that the main trait of the "dispersionless transport" is actually not the plateau of the dispersion, but its wild fluctuations within the plateau region (inset in Fig. 3.1 and right inset in Fig. 3.2). It is the dispersion fluctuations that prevent one from determining the diffusion coefficient numerically. They have to do with the finite sampling size used in any simulations. We also showed that it is possible to measure the diffusion coefficient within the plateau regime (Fig. 3.3) by a small modification of the measurement procedure described in Chapter 3 and shown to work for the parameters which were problematic in the original paper by Lindenberg et al [2].

The emergence of the long-flight phenomenon (Lévy flight) at high temperatures in the SHOC model, leading to the breakdown of the Einstein relation, is attributed to the dissipative force being a decreasing function of the particle velocity. To explore the breakdown of the Einstein relation, we performed our third investigation of the model of a free BP with velocity-dependent damping. This model is simple enough to allow for an analytical determination of the diffusion coefficient D. It is revealed that at high temperatures, the emergence of long flights and the non-linear correlation between D and T critically depend on the velocity dependence of the damping function. In the case where the damping function $\gamma(v)$ decreases as a finite power of the particle's kinetic energy, i.e., $\gamma(v) \propto 1/v^{2\alpha}$, a non-linear relation, $D \propto T^{\alpha+1}$, is observed; however, the long flight events are absent (Fig. 4.1 (b), (c)). In contrast, if damping is given by a Gaussian function, $\gamma(v) \propto e^{-v^2}$, for the temperatures below a critical value T_c, the diffusion coefficient follows a scaling relationship of $D \propto 1/\sqrt{T_c - T}$. However, for temperatures exceeding T_c, the particle exhibits superdiffusive motion characterized by long flight events in its trajectory (Fig. 4.1 (e), (f)).

Remarkably, in this regime, the diffusion coefficient diverges, showcasing a non-Einsteinian relation between D and T with an infinite diffusion coefficient. Our analytical formula is confirmed by numerical simulations.

5.2 Future work

Although this thesis has provided significant insights into the behavior of 1D Brownian motion in the three models mentioned above, there are still some aspects that remain unexplored and can be investigated in future work. Here are a few potential directions for future research:

1. Multi-dimensional extension: While this thesis has focused on 1D Brownian motion, a natural extension is to explore the behavior of BPs in higher dimensions [3–5]. We believe our MSBC algorithm can be modified to study two and three dimensional generalizations of the SHOC model.

2. More than one BP interacting with heat bath: it is interesting to consider the behaviour of two or more BPs on a SHOC or other models in one or more dimensions. It is expected that even in the absence of the direct particle-particle interaction, the heat bath will serve as a mediator through which the particles will "feel" each other.

3. Experimental validation: While the models studied in this thesis have been validated through theoretical analysis and simulations, experimental validation of the theoretical predictions would be a significant contribution. For example, experimental studies of Brownian motion in carbon nanotubes could provide valuable insights into the behavior of BP/SHOC model [6, 7].

4. Other damping functions: The thesis has investigated the behavior of BPs with a specific form of velocity-dependent damping function. However, there are many other

forms of damping functions that could be explored in future research. Investigating the behavior of BPs under different damping functions could reveal new insights into the fundamental physics of Brownian motion.

5. Deterministic systems: Investigation of Brownian motion on deterministic non-linear systems, in which stochastisity arises due to the onset of chaotic dynamics [8–12], such as the Fermi-Pasta-Ulam chain.

6. Real-life systems: Another interesting future research possibility can be modeling adatom diffusion on solid surfaces, which would contribute to a better understanding of the dynamics and behavior of adatoms in real-life systems [13, 14].

Overall, the examined models in this thesis provide a basis for future research on transport phenomena in a wide range of physical systems. The power laws and scaling relationships observed in our studies can be tested and applied to a variety of other systems. Therefore, future research in this field will provide valuable insights into transport phenomena in diverse physical systems.

Bibliography

[1] M. Evstigneev and A. Al-Haidari, Brownian motion on a stochastic harmonic oscillator chain: limitations of the Langevin equation. *J. Phys. A: Math. Theor.*, **52**, 055001, (2019).

[2] K. Lindenberg, J.M. Sancho, A.M. Lacasta, and I.M. Sokolov, Dispersionless transport in a washboard potential. *Phys. Rev. Lett.*, **98**, 020602, (2007).

[3] C. Baldock, P. J. Harris, A. R. Piercy and B. Healy, Experimental determination of the diffusion coefficient in two-dimensions in ferrous sulphate gels using the finite element method. *Australas. Phys. and Eng. Sci. Med.*, **24**, 19, (2001).

[4] S. Babic, J. Battista and K. Jordan, Radiochromic leuco dye micelle hydrogels: II. Low diffusion rate leuco crystal violet gel. *Phys. Med. Biol.*, **54**, 6791, (2009).

[5] K. N. Dzhumagulova, T. S. Ramazanov, and R. U. Masheeva, Diffusion coefficient of three-dimensional Yukawa liquids. *Phys. of Plas.*, **20**, 113702, (2013).

[6] M. Melillo, F. Zhu, M.A. Snyder, and J. Mittal, Water transport through nanotubes with varying interaction strength between tube wall and water. J. Phys. Chem. Lett. **2**, 2978, (2011).

[7] J. Geng et al., Stochastic transport through carbon nanotubes in lipid bilayers and live cell membranes. *Nature* **514**, 612, (2014).

[8] P. Jung, J. G. Kissner, and P. Hänggi, Regular and Chaotic Transport in Asymmetric Periodic Potentials: Inertia Ratchets. *Phys. Rev. Lett.*, **76**, 3436, (1996).

[9] J. L. Mateos, Chaotic Transport and Current Reversal in Deterministic Ratchets. *Phys. Rev. Lett.*, **84**, 258, (2000).

[10] M. Borromeo, G. Costantini, and F. Marchesoni, Deterministic ratchets: Route to diffusive transport. *Phys. Rev. E.*, **65**, 041110, (2002).

[11] J. L. Mateos, Current reversals in chaotic ratchets: the battle of the attractors. *Physica A*, **325**, 92, (2003).

[12] F. R. Alatriste and J. L. Mateos, Anomalous mobility and current reversals in inertial deterministic ratchets. *Physica A*, **384**, 223, (2007).

[13] K.-D. Shiang, Molecular dynamics simulation of adatom diffusion on metal surfaces. *J. Chem. Phys.*, **99**, 9994, (1993).

[14] E. El koraychy, K. Sbiaai, M. Mazroui, R. Ferrando and Y. Boughaleb, Heterodiffusion of Ag adatoms on imperfect Au(110) surfaces. *Chem. Phys. Lett.*, **669**, 150-155, (2017).